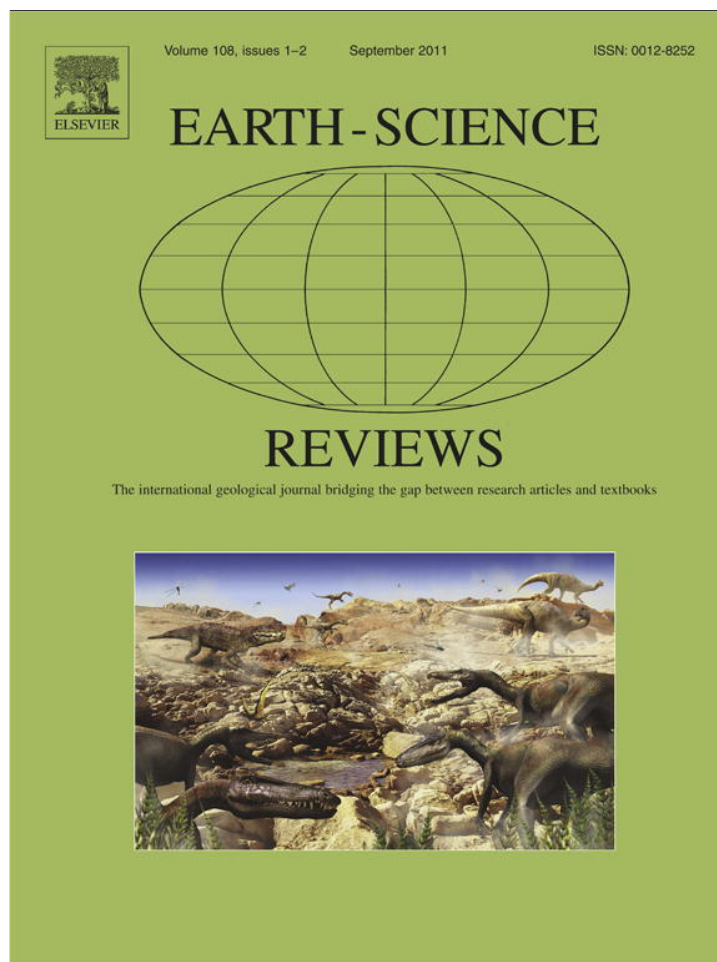


Provided for non-commercial research and education use.
Not for reproduction, distribution or commercial use.



This article appeared in a journal published by Elsevier. The attached copy is furnished to the author for internal non-commercial research and education use, including for instruction at the authors institution and sharing with colleagues.

Other uses, including reproduction and distribution, or selling or licensing copies, or posting to personal, institutional or third party websites are prohibited.

In most cases authors are permitted to post their version of the article (e.g. in Word or Tex form) to their personal website or institutional repository. Authors requiring further information regarding Elsevier's archiving and manuscript policies are encouraged to visit:

<http://www.elsevier.com/copyright>



Contents lists available at ScienceDirect

Earth-Science Reviews

journal homepage: www.elsevier.com/locate/earscirev

Secular trends in the geologic record and the supercontinent cycle[☆]

Dwight C. Bradley^{*}

U.S. Geological Survey, 4200 University Drive, Anchorage, AK 99508, USA

ARTICLE INFO

Article history:

Received 13 July 2010

Accepted 17 May 2011

Available online 26 May 2011

Keywords:

Supercontinent

Secular trends

Time series

Precambrian geology

Passive margin

Detrital zircon

ABSTRACT

Geologic secular trends are used to refine the timetable of supercontinent assembly, tenure, and breakup. The analysis rests on what is meant by the term *supercontinent*, which here is defined broadly as a grouping of formerly dispersed continents. To avoid the artificial pitfall of an all or nothing definition, quantitative measures of “supercontinentality” are presented: the number of continents, and the area of the largest continent, which both can be gleaned from global paleogeographic maps for the Phanerozoic. For the secular trends approach to be viable in the deep past when the very existence of supercontinents is debatable and reconstructions are fraught with problems, it must first be calibrated in the Phanerozoic against the well constrained Pangea supercontinent cycle. The most informative geologic variables covering both the Phanerozoic and Precambrian are the abundances of passive margins and of detrital zircons. Both fluctuated with size of the largest continent during the Pangea supercontinent cycle and can be quantified back to the Neoproterozoic. The tenure of Pangea was a time represented in the rock record by few zircons and few passive margins. Thus, previously documented *minima* in the abundance of detrital zircons (and orogenic granites) during the Precambrian (Condie et al., 2009a, *Gondwana Research* 15, 228–242) now can be more confidently interpreted as marking the tenures of supercontinents. The occurrences of carbonatites, granulites, eclogites, and greenstone belt deformation events also appear to bear the imprint of Precambrian supercontinent cyclicity. Together, these secular records are consistent with the following scenario. The Neoproterozoic continental assemblies of Superia and Sclavia broke up at ca. 2300 and ca. 2090 Ma, respectively. Some of their fragments collided to form Nuna by about 1750 Ma; Nuna then grew by lateral accretion of juvenile arcs during the Mesoproterozoic, and was involved in a series of collisions at ca. 1000 Ma to form Rodinia. Rodinia broke up in stages from ca. 1000 to ca. 520 Ma. Before Rodinia had completely come apart, some of its pieces had already been reassembled in a new configuration, Gondwana, which was completed by 530 Ma. Gondwana later collided with Laurentia, Baltica, and Siberia to form Pangea by about 300 Ma. Breakup of Pangea began at about 180 Ma (Early Jurassic) and continues today. In the suggested scenario, no supercontinent cycle in Earth history corresponded to the ideal, in which *all* the continents were gathered together, then broke apart, then reassembled in a new configuration. Nuna and Gondwana ended their tenures not by breakup but by collision and name change; Rodinia's assembly overlapped in time with its disassembly; and Pangea spalled Tethyan microcontinents throughout much of its tenure. Many other secular trends show a weak or uneven imprint of the supercontinent cycle, no imprint at all. Instead, these secular trends together reveal aspects of the shifting background against which the supercontinents came and went, making each cycle unique. Global heat production declined; plate tectonics sped up through the Proterozoic and slowed down through the Phanerozoic; the atmosphere and oceans became oxidized; life emerged as a major geochemical agent; some rock types went extinct or nearly so (BIF, massif type anorthosite, komatiite); and other rock types came into existence or became common (blueschists, bioclastic limestone, coal).

Published by Elsevier B.V.

Contents

1. Introduction	17
2. What constitutes a supercontinent?	18
3. Pangea.	19
4. Secular trends that reflect the supercontinent cycle.	19
4.1. Area of the largest continent and number of continents	19

[☆] Bradley, D.C., 2011. Secular trends in the geologic record and the supercontinent cycle. *Earth-Science Reviews* ##, ##-##.

^{*} Tel.: +1 907 786 7434; fax: +1 907 786 7401.

E-mail address: dbradley@usgs.gov.

4.2.	Abundance, start dates, and end dates of passive margins	20
4.3.	Granites and detrital zircons	24
4.4.	Isotopic composition of seawater strontium	26
4.5.	Deformation ages of greenstone belts	26
4.6.	Eclogite and granulite facies metamorphism	26
4.7.	Carbonatites	27
4.8.	Large igneous provinces	27
5.	Proposed supercontinent timetable	27
5.1.	Vaalbara, Superia, and Sclavia (Bleeker, 2003) or Kenorland (Williams et al., 1991)	27
5.2.	Nuna	27
5.3.	Rodinia	28
5.4.	Gondwana	28
6.	Supercontinent cycles and other secular variation	28
6.1.	Global heat production and rates of plate tectonics	28
6.2.	Oceanic crust and passive margin proxies	29
6.3.	Obducted ophiolites	29
6.4.	High pressure, low temperature metamorphic rocks	29
6.5.	Mantle derived igneous rocks	29
6.6.	Massif type anorthosites	30
6.7.	Orogenic gold deposits	30
6.8.	Sedimentary rocks	30
6.9.	Sedimentary recycling	30
6.10.	Oxygenation of the atmosphere and oceans	30
6.11.	Glaciation	31
6.12.	Sea level	31
6.13.	Mississippi Valley type lead zinc deposits	31
6.14.	Other secular trends	31
7.	Summary	31
	Acknowledgments	32
	Appendix A. Supplementary data	32
	References	32

1. Introduction

Global paleogeography and plate interactions are reasonably well understood back to the assembly of Pangea in the late Paleozoic (Fig. 1). Multiple lines of evidence go into these reconstructions: marine magnetic anomalies, passive margin matchups, geologic interpretation of orogenic belts, paleomagnetism, paleobiogeography of fossils, and distribution of climatically sensitive strata and the results are synthesized into a scenario that is consistent with the rules of plate kinematics. Like genealogy, however, the plate reconstruction approach to Earth history gets harder and harder back through time, as each trail of evidence gets fainter. It would be pointless, for example, to attempt a *global* plate reconstruction at 4030 Ma, with only the Acasta Gneiss to go on. Precambrian reconstructions are easiest when continents were clustered together and there were fewer objects; but even these times of supercontinent tenure are a challenge. For example, Neoproterozoic reconstructions of Rodinia (Moore, 1991; Karlstrom et al., 2001; Li et al., 2008; Evans, 2009) show West Africa in very different positions. If it is that hard to decide where it goes, the assumption that West Africa was part of a Rodinia supercontinent is itself open to question.

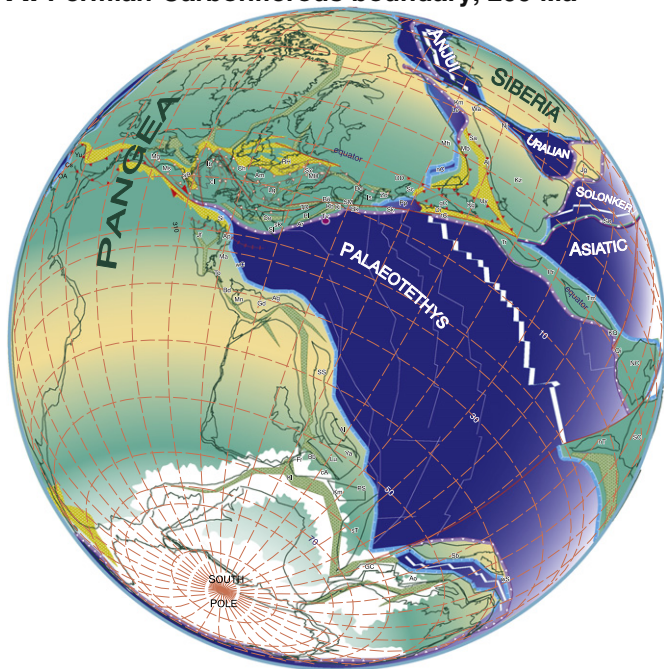
A complementary approach to Earth history is the analysis of secular trends (e.g., Condie, 2005; Dewey, 2007; Reddy and Evans 2009; Condie et al., 2011; Goldfarb et al., 2010). Countless geologic variables can be tracked through time, even times when plate reconstructions are out of the question. This makes it possible to sidestep the unknown specifics of plate paleogeography and instead focus on evolution of the Earth system as a whole. Two precepts guide this approach: (1) every secular trend can have only one correct explanation (complicated though it might be); and (2) any viable explanation for one secular trend must honor all the rest.

The supercontinent cycle (Fig. 2) is manifested in a number of secular trends (e.g., Worsley et al., 1984, 1986; Nance et al., 1986;

Barley and Groves, 1992; Condie, 2005; Condie et al., 2009a; Hawkesworth et al., 2010) and is well suited to study by this means because the opening and closing of ocean basins impact many parts of the Earth system. In this paper, I examine the timing of past supercontinent cycles using a new compilation of secular trends for most of the geologic datasets for which this sort of information is now available: age distributions of rocks and minerals, geochemical trends, censuses of tectonic settings, numerical model results, and more. Many new global secular trends are published every year. The most informative secular trends for present purposes are those that show fluctuations related to the assembly, tenure, and disassembly of Pangea. It will be shown that the tenure of Pangea was a time of few passive margins and low zircon abundance. These two variables can be tracked deeper into the past to deduce, on uniformitarian grounds, the tenures of putative Precambrian supercontinents. A number of secular trends show this same irregular pulse, with maxima and minima at several hundred million years' spacing (Figs. 11–23). Other secular trends show little or no sign of it, however, but instead paint a changing backdrop against which the supercontinents have come and gone (Figs. 24–45).

The terms “secular trend”, “time trend”, and “time series” are used here as synonyms for a set of ordered pairs (x, y) where y is a geologic variable and x is its age. The new compilation expands on previous compendia of secular trends by Garrels and Mackenzie (1971), Meyer (1981, 1988), Nance et al. (1986), Hallam (1992), Barley and Groves (1992), Groves et al. (2005), Condie (1997, 2005), and Veizer and Mackenzie (2003). A few plots are new, either constructed from data that were given only in tabular form in the original publications, or from my own compilations. The plots are divided between the main body of the paper (Figs. 3–45; Table 1) and a Supplementary data section (Figs. A1–A86; Table A1), available online. Tables 1 and A1 serve as figure captions. The Supplementary data section includes discussions of the data or model assumptions behind some plots.

A. Permian–Carboniferous boundary, 299 Ma



B. Late Jurassic, 156 Ma

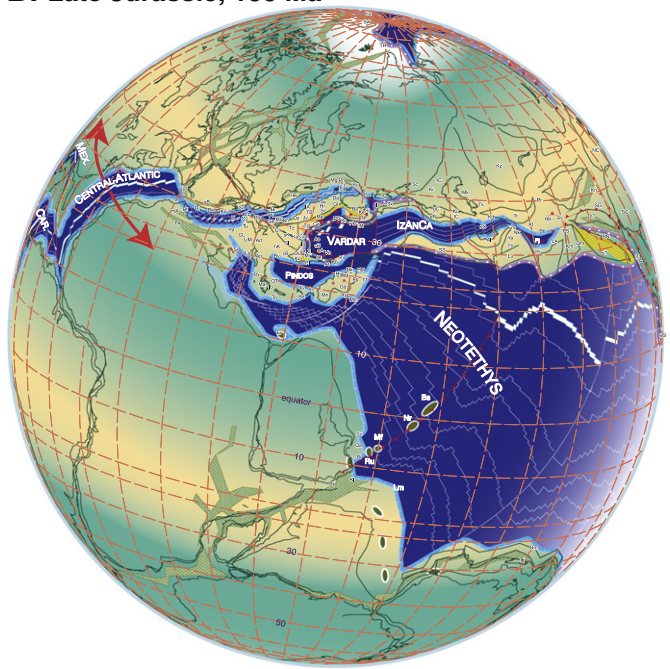


Fig. 1. Paleogeographic plate reconstructions from Stampfli and Borel (2002). (A) Permian–Carboniferous boundary, about 299 Ma. Pangea is in its final stages of assembly. Although roughly 95% of the continental area was in Pangea, a series of microcontinents dotted the Paleotethyan ocean, in transit from Gondwana to Eurasia. (B) Late Jurassic, about 156 Ma. The main Pangean landmass is shown in an early stage of breakup. On a constant-radius Earth, opening of the central Atlantic between Africa and North America (red arrows) must have been accompanied by the subduction of an equivalent amount of seafloor, most likely along North America's Cordilleran margin.

All secular trends have been plotted or replotted with time as the x axis and the present on the left¹. Plots are presented at two time scales, either covering the Phanerozoic plus the very end of the Neoproterozoic (550 Ma to present), or spanning Earth history in its entirety (4560 Ma to present). Numerical age assignments use the time scale of Gradstein and Ogg (2004), except for a few plots that have an older time scale inextricably embedded in the construction.

2. What constitutes a supercontinent?

Multiple lines of evidence suggest that there have been times when some formerly independent continents came together, and other times when larger continents fragmented into smaller ones. When is a grouping of continents big enough to earn the name *supercontinent*? Does this semantic distinction even matter? Many tectonicists use the term *supercontinent* in the sense of Hoffman (1999): “a clustering of nearly all the continents” or Rogers and Santosh (2003): “an assembly of all or nearly all the Earth's continental blocks”. I suggest that an “all or nearly all” definition (1) sets the bar higher than the rock record requires, and (2) is impossible to rigorously apply in the Precambrian, when plate reconstructions are equivocal. Some researchers treat Gondwana as one of the supercontinents (e.g., Condie 2005; Korenaga, 2006) but it fails to meet the “all or nearly all” definition, because it didn't include Siberia, Baltica, or Laurentia, it became Pangea. Bleeker (2003) coined the term *supercraton* for clusters of continents that would not meet the “all or nearly all” requirement. I prefer a more inclusive definition of *supercontinent*: a grouping of formerly dispersed continents. The difference between the “all or nearly all” and “inclusive” definitions is more than just semantics, because it bears on whether or not the

¹ This is now the universal convention in detrital zircon geochronology, the subdiscipline that accounts for the vast majority of geologic time series now being published.

supercontinent cycle is periodic (as suggested by Korenaga, 2006, among others) or stochastic. What is ultimately needed is a numerical index of “supercontinentality”, as discussed further in Section 4.1.

A single round of the *supercontinent cycle* refers to the Earth as a whole and involves the breakup of one supercontinent and the subsequent assembly of a new one. A corollary of the inclusive definition is the allowance that all the same pieces need not be parts of both the first supercontinent and the second. Indeed, as noted by Bleeker (2003), no supercontinent cycle in Earth history can be proven to have conformed to the ideal cycle, with *all* of the continents gathered into one, then breakup, and then reassembly of *all* of the pieces into some new configuration.

The terms “supercontinent cycle” and “Wilson cycle” are not synonymous. The Wilson cycle² refers to the opening and closing of a single ocean basin. Despite a widespread misconception, there is no stipulation in a Wilson cycle that the continent that rifts away is the one that comes back; indeed this appears to be the rare case. A supercontinent cycle is global and involves the aggregate effect of many Wilson cycles that are only roughly synchronous. The timing of a Wilson cycle can be closely specified. The start date is when seafloor spreading begins during the separation of two continents, and the end date is when the last of this seafloor is consumed during collision. The timing of a supercontinent cycle as a whole can't be easily specified because the component Wilson cycles aren't perfectly synchronized.

Hypothetical scenarios for supercontinent evolution are shown in Fig. 2. The more straightforward scenario (Fig. 2A E) corresponds to what Murphy and Nance (2003, 2007) referred to as *extroversion*: the supercontinent turns “inside out” (Hoffman, 1991). Supercontinent #1 breaks up, and the pieces eventually regroup elsewhere in a completely new configuration as supercontinent #2. In Fig. 2A C, breakup of supercontinent #1 is enabled by subduction along two

² The concept was first elaborated by Wilson (1968); the name was coined by Dewey and Burke (1974).

Andean type margins, much as the opening of the Atlantic during Pangea's breakup was accompanied by Cordilleran subduction along the Pacific rim during the Mesozoic (Collins, 2003). After the supercontinent splits in two, each succeeding frame follows naturally from the one before, eventually leading to formation of supercontinent #2 on the other side of the globe.

The more complex, hypothetical case known as *introversion* is shown in Fig. 2F–J. Supercontinent #1 breaks up, and its pieces move apart for some distance but then reverse course and collide to form supercontinent #2 in about the same place as before. During the reversal, two subduction zones and a spreading center must die, and two new subduction zones and a spreading center must be born.

3. Pangea

Pangea is the most recent and best understood supercontinent. Its basic configuration was appreciated a century ago by the early proponents of continental drift, Taylor and Wegener. Pangea's late Paleozoic to early Mesozoic tenure (ca. 310 to 180 Ma) is well constrained. Working back from the present, Pangea is reconstructed simply by fitting the continents that border Atlantic type oceans: Europe, Greenland, Africa, North America, India, Antarctica, Australia, Antarctica, and so on.

The Pangea fit also has to account for continents that migrated south to north across Paleothethys and Neothethys during the late Paleozoic and Mesozoic (Fig. 1) (e.g., Sengör et al., 1988; Stampfli et al., 1991; Stampfli and Borel, 2002). In the absence of marine magnetic anomalies, this part of the puzzle relies on the art of deciphering orogenic belts. The Tethyan continents are what keep Pangea from being an “ideal” supercontinent: it *never* contained all of the continental crust.

4. Secular trends that reflect the supercontinent cycle

4.1. Area of the largest continent and number of continents

Although differing in detail, all published Phanerozoic plate reconstructions (e.g., Scotese, 1997; Stampfli and Borel, 2002) plainly show that the continents were dispersed, then gathered together, and then dispersed once again. Two secular trends, derived for the present study from the maps of Scotese (1997), serve as quantitative indices of “supercontinentality”.

In Fig. 3 10, the area of the largest single continent was tracked through time by summing the areas of the main pieces, using values of continental areas from Cogley (1984). Today, there are five major continental masses: South America, Africa, Australia, Antarctica, and the largest one, Eurasia plus North America. The latter two are joined across the logjam of Phanerozoic accreted terranes in Alaska and the Russian Far East, and I count them as one (even though they are kinematically separate plates) because their mutual boundary is long, diffuse, and relative motions are extremely slow. I count Arabia and India as part of Eurasia on the grounds that the Himalayan and Zagros sutures have long since closed, and I count Greenland with North America because the two never completely separated and are no longer in relative motion. North America and South America are considered separate for this analysis, because even though they are presently linked by a narrow arc, the connection appears to be ephemeral; if they appeared in the same relative positions in an older reconstruction, they would certainly be treated as separate. Working back through time, the same kinds of decisions are needed for each time slice but with less information; the resulting time trend (Fig. 3 10) is subjective in detail, though certainly correct in broad form.

A related way of tracking supercontinent assembly and disassembly in the Phanerozoic is by the number of independent continents (Fig. 4). The trouble is that every continent counts as one regardless of size, and the size cutoff for whether or not to count a microcontinent is arbitrary. Two versions of this time trend are shown, one from Worsley et al.

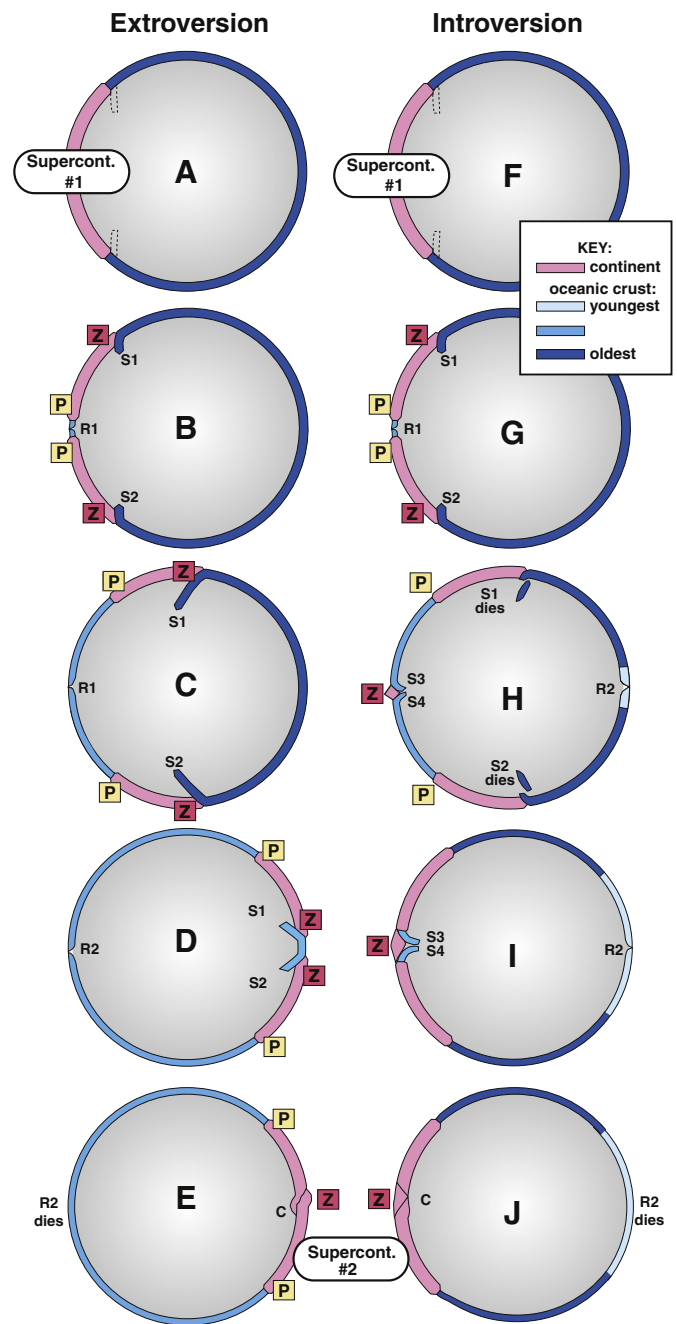
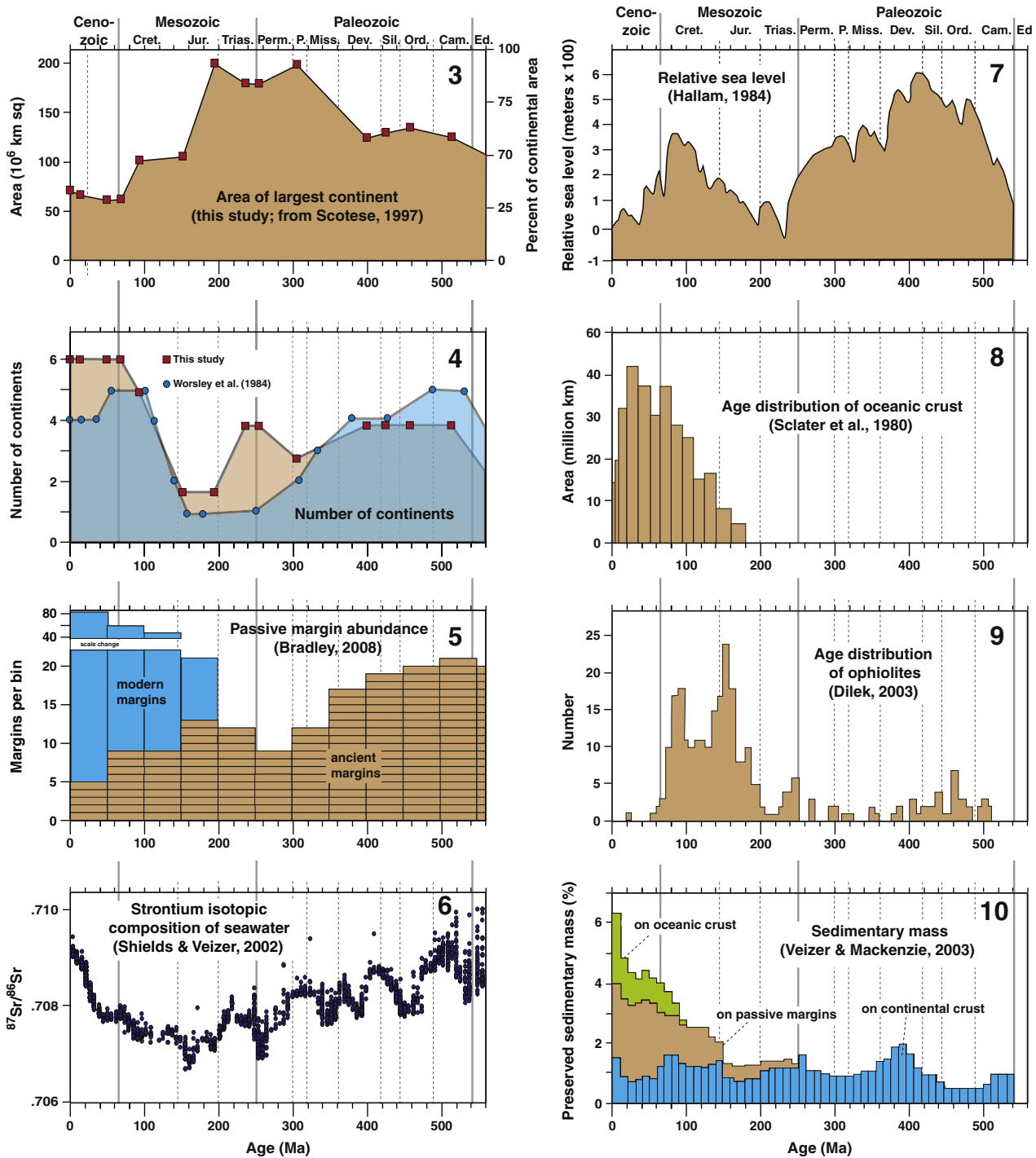


Fig. 2. Schematic cross sections through the Earth showing two idealized modes of supercontinent cyclity, showing many of the same concepts as a figure of Silver and Behn (2008). Passive margins related to each cycle are indicated by a “P” and zircon-forming environments by a “Z”. R1 and R2 identify spreading ridges; S1 to S4 identify subduction zones; C indicates collisional orogens. In order to emphasize only those plate motions directly involved in the supercontinent cycle, preexisting plate boundaries are not shown in the first frame of each sequence; the simplest scenarios would commence with subduction zones already in existence, as indicated by the dashed slabs in A and F. (A–E) Extroversion. Breakup of supercontinent #1 is enabled by subduction along two Andean-type margins (S1 and S2). The two halves of supercontinent #1 eventually collide (C) on the other side of the world to form supercontinent #2. (F–J) Introversion. At first, the sequence is the same as for extroversion, but in order to return to where they began, the two diverging continents somehow must reverse course. This implies that the two original subduction zones (S1 and S2) must die, that the seafloor that formed at spreading center R1 must now be consumed at one or more new subduction zones (e.g., S3 and S4), and that one new spreading ridge (R2) must appear.



Figs. 3-10. Secular trends for 0 to 550 Ma. (Table 1 takes the place of these captions).

(1984) and the other derived for the present study from the reconstructions of Scotese (1997). Whereas the time trends differ in detail, the tenure of Pangea corresponds to a broad minimum in both plots.

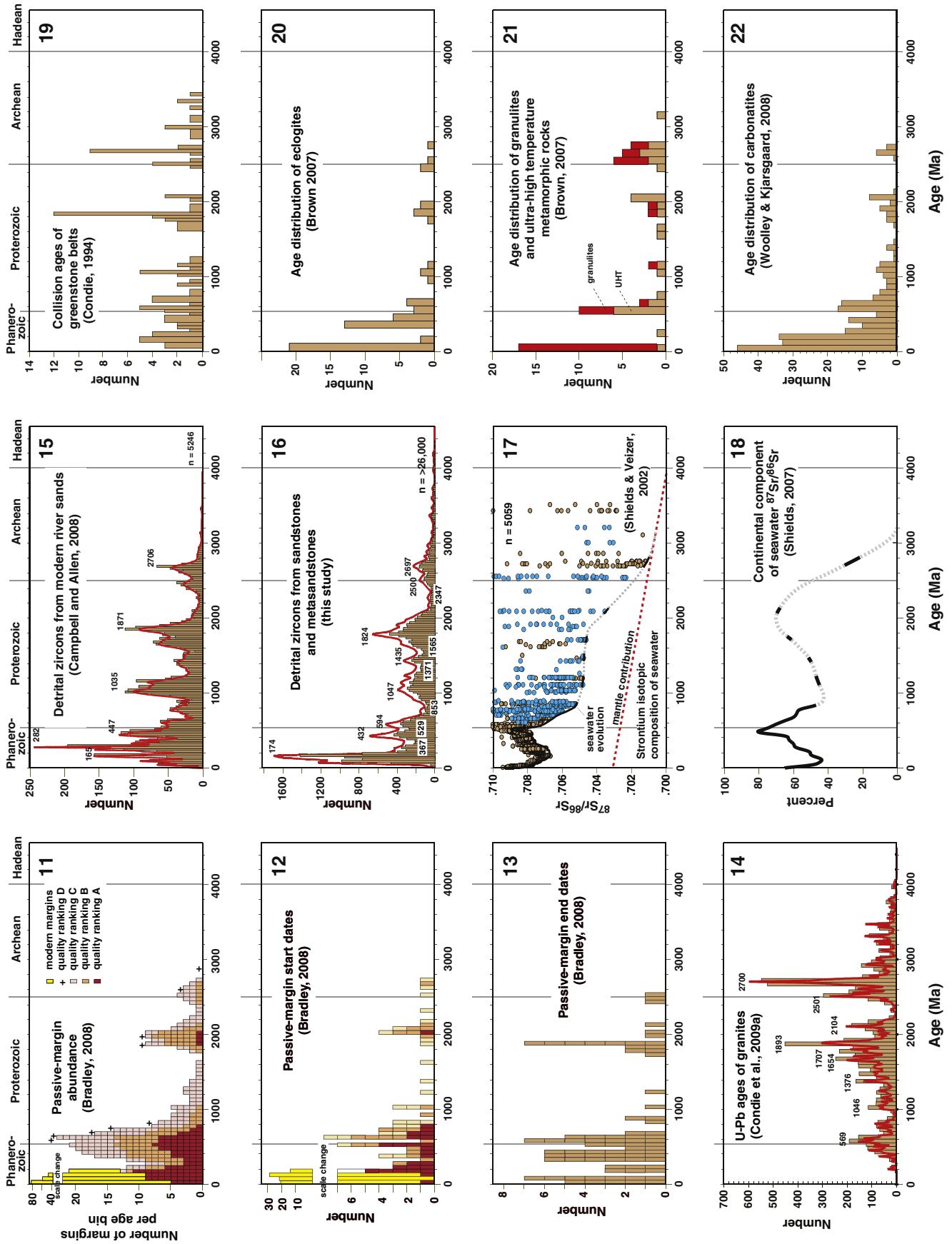
Precambrian plate reconstructions are not nearly as robust as Phanerozoic ones, so quantitative measures of “supercontinentality” area of the largest continent and number of continents are fraught with uncertainty. Proxies are needed.

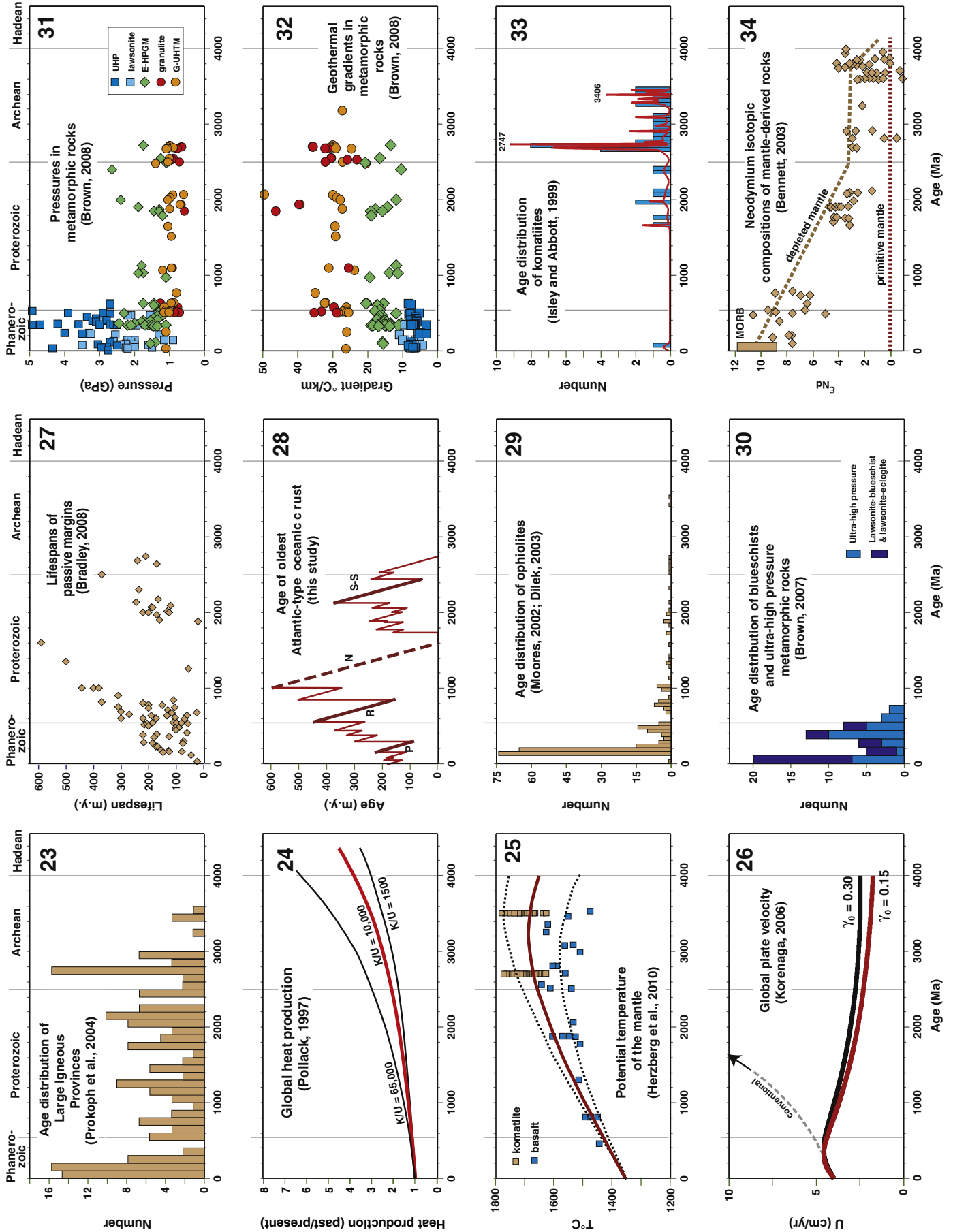
4.2. Abundance, start dates, and end dates of passive margins

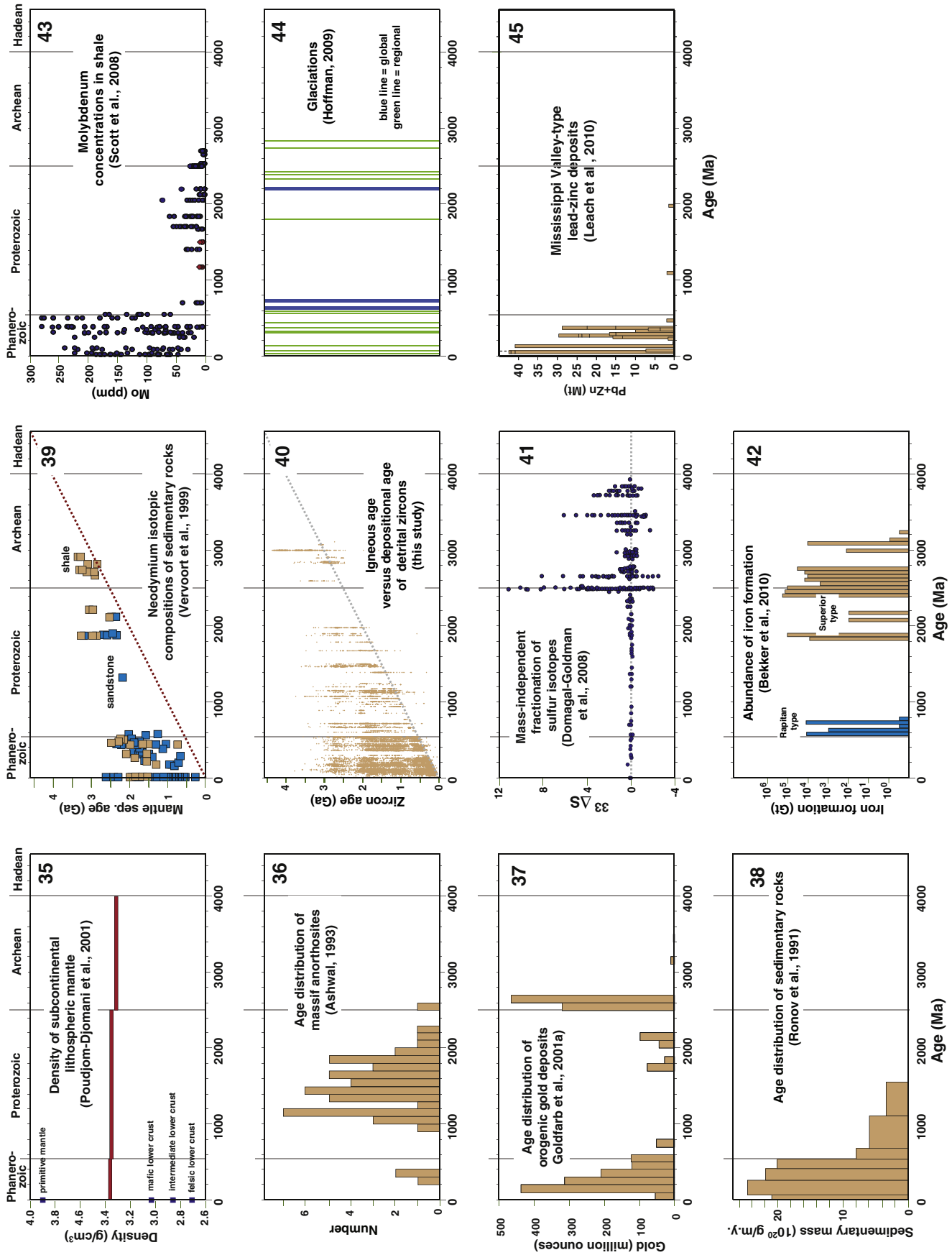
Passive margins form along the matching edges of continents that rift and are then carried apart by seafloor spreading. The supercontinent

cycle controls the global abundance of passive margins, because passive margins are created during supercontinent breakup and are destroyed during supercontinent assembly (Fig. 2). The present day passive margins those flanking extant Atlantic type oceans total about 100,000 km in length and range in age from a few million years (Red Sea) to about 180 million years (east coast of Africa). Analysis of ancient passive margins is not as straightforward because they no longer face an ocean, but instead are preserved in orogenic belts (Bradley, 2008).

The Phanerozoic age distribution of passive margins (Fig. 46) tracks the assembly, tenure, and disassembly of Pangea. The tenure of Pangea coincided with a low at 300 to 275 Ma. The increase in passive margins since then tracks Pangea’s breakup; the sharp decline from ca. 500 to







Figs. 11–45. Secular trends for 0 to 4560 Ma. (Table 1 takes the place of these captions).

Table 1
Summaries of time-series plots in Figs. 3–43.

Fig. no.	Variable	Time span (Ma)	Reference and comments
3	Area of largest continent	0–550	This study, derived from Scotese (1997)
4	Number of continents	0–550	This study and Worsley et al. (1984)
5	Passive margin abundance	0–550	Bradley (2008)
6	Strontium isotopic composition of seawater	0–550	Shields and Veizer (2002)
7	Relative sea level	0–550	Hallam (1992); similar to the curve by Haq et al. (1987) and Haq and Schutter (2008) but constructed on different principles
8	Age distribution of oceanic crust	0–550	Slater et al. (1980)
9	Age distribution of ophiolites	0–550	Dilek (2003)
10	Sedimentary mass	0–550	Veizer and Mackenzie (2003) using a plot from Hay
11	Passive-margin abundance	0–4560	Bradley (2008)
12	Passive-margin start dates	0–4560	Bradley (2008)
13	Passive-margin end dates	0–4560	Bradley (2008)
14	U–Pb ages of granites	0–4560	Condie et al. (2009a)
15	Detrital zircons from modern river sands	0–4560	Campbell and Allen (2008); a similar plot was published by Rino et al. (2008)
16	Detrital zircons from sandstones and metasandstones	0–4560	This study
17	Strontium isotopic composition of seawater	0–4560	Shields and Veizer, 2002
18	Continental component of seawater $^{87}\text{Sr}/^{86}\text{Sr}$	0–4560	Shields (2007)
19	Collision ages of greenstone belts	0–4560	Condie (1994)
20	Age distribution of eclogites	0–4560	Brown (2007); medium T eclogite–high P granulite
21	Age distribution of granulites and ultra-high temperature metamorphic rocks	0–4560	Brown (2007)
22	Age distribution of carbonates	0–4560	Woolley and Kjarsgaard (2008)
23	Age distribution of Large Igneous Provinces	0–4560	Prokoph et al. (2004)
24	Global heat production	0–4560	Pollack (1997). Red curve shows favored mix of radioactive fuels.
25	Potential temperature of the mantle	0–4560	Herzberg et al. (2010). Curves represent model calculations based on different Urey ratios.
26	Global plate velocity	0–4560	Korenaga (2006). Black and red curves represent different Urey ratios.
27	Lifespans of passive margins	0–4560	Bradley (2008)
28	Age of oldest Atlantic-type oceanic crust	0–4560	Bradley (2008) and this study. Dashed segment is poorly constrained.
29	Age distribution of ophiolites	0–4560	Dilek (2003); Moores (2002)
30	Age distribution of blueschists and ultra-high pressure metamorphic rocks	0–4560	Brown (2007)
31	Pressures in metamorphic rocks	0–4560	Brown (2008)
32	Geothermal gradients in metamorphic rocks	0–4560	Brown (2008)
33	Age distribution of komatiites	0–4560	Pollack (1997)
34	Neodymium isotopic compositions of mantle-derived rocks	0–4560	Bennett (2003)
35	Density of subcontinental lithospheric mantle	0–4560	Poudjom Djomani et al. (2001)
36	Age distribution of massif anorthosites	0–4560	Ashwal (1993)
37	Age distribution of orogenic gold deposits	0–4560	Goldfarb et al. (2001a)
38	Age distribution of sedimentary rocks	0–4560	Ronov et al. (1991)
39	Neodymium isotopic compositions of sedimentary rocks	0–4560	Vervoort et al. (1999)
40	Igneous age versus depositional age of detrital zircons	0–4560	This study
41	Mass-independent fractionation of sulfur isotopes	0–4560	Domagal-Goldman et al. (2008)
42	Abundance of iron formation	0–4560	Bekker et al. (2010)
43	Molybdenum concentrations in shale	0–4560	Scott et al. (2008)
44	Glaciations	0–4560	Hoffman (2009) and unpublished
45	Mississippi Valley-type lead-zinc deposits	0–4560	Leach et al. (2010)

ca. 350 Ma coincides with Pangea's assembly. Thus the Phanerozoic portion of the passive margin age distribution forms a clear pattern with a straightforward connection to the Pangea supercontinent cycle.

Deeper in the past (Fig. 11), the abundance of passive margins increased between ca. 2750 and 2500, between ca. 2300 and 2050, and between ca. 1050 and 650 Ma, and it declined from ca. 2500 to 2400 and ca. 1850 to 1750; these times bracket lows at ca. 2400–2300 and ca. 1750–1650 Ma (Bradley, 2008). There is no evidence that the uneven age distribution is primarily due to uneven preservation. Instead, applying the patterns from the Phanerozoic, the fluctuations are inferred to mark times of supercontinent disassembly, assembly, and tenure, respectively. Superimposed on the various fluctuations, the passive margin age distribution is dominated by younger margins, which I attribute to a combination of destruction of older margins, difficulties in recognizing and dating the vestiges of old margins in ancient orogens, and different counting conventions between modern and ancient margins (Bradley, 2008). The utility of passive margin abundance as a proxy for supercontinent cycles hinges on the accuracy and thoroughness of the census, as discussed further in the Supplementary data section.

The start dates and end dates of these passive margins are shown in Figs. 12 and 13. The start date of a passive margin is taken as the onset of seafloor spreading (i.e., the rift drift transition) (Bradley,

2008). Maxima in this plot at 2050, 2000, 650, 600, 550, 500, and 150–100 Ma represent times of synchronized continental breakup. For the vast majority of passive margins that met their end by colliding with a convergent margin, the end date is taken as the time when the continent–ocean boundary entered the subduction zone at the start of arc passive margin collision. Maxima are at 1850, 1800, 600, 550, 450, 300, and 100–50 Ma. Each start date and each end date represents a plate reorganization involving the formation or death of a divergent plate boundary and the formation or death of a convergent plate boundary (cf. Fig. 2). The broad age distributions in Figs. 12 and 13 are similar but slightly offset, as would be expected.

4.3. Granites and detrital zircons

Condie et al. (2009a) showed that granites and detrital zircons that were ultimately derived from them have remarkably similar, strongly episodic age distributions. The fluctuations have been interpreted in terms of Precambrian supercontinent cycles (e.g., Condie et al., 2009a). Both granites and detrital zircons have advantages and shortcomings for this line of inquiry. U–Pb zircon ages of granites specifically, those classed as orogenic granites (Condie et al., 2009a) provide the more direct record. The recent global census of igneous U–Pb ages by Condie et al. (2009a) is shown in Fig. 14. The robust, Precambrian part of this

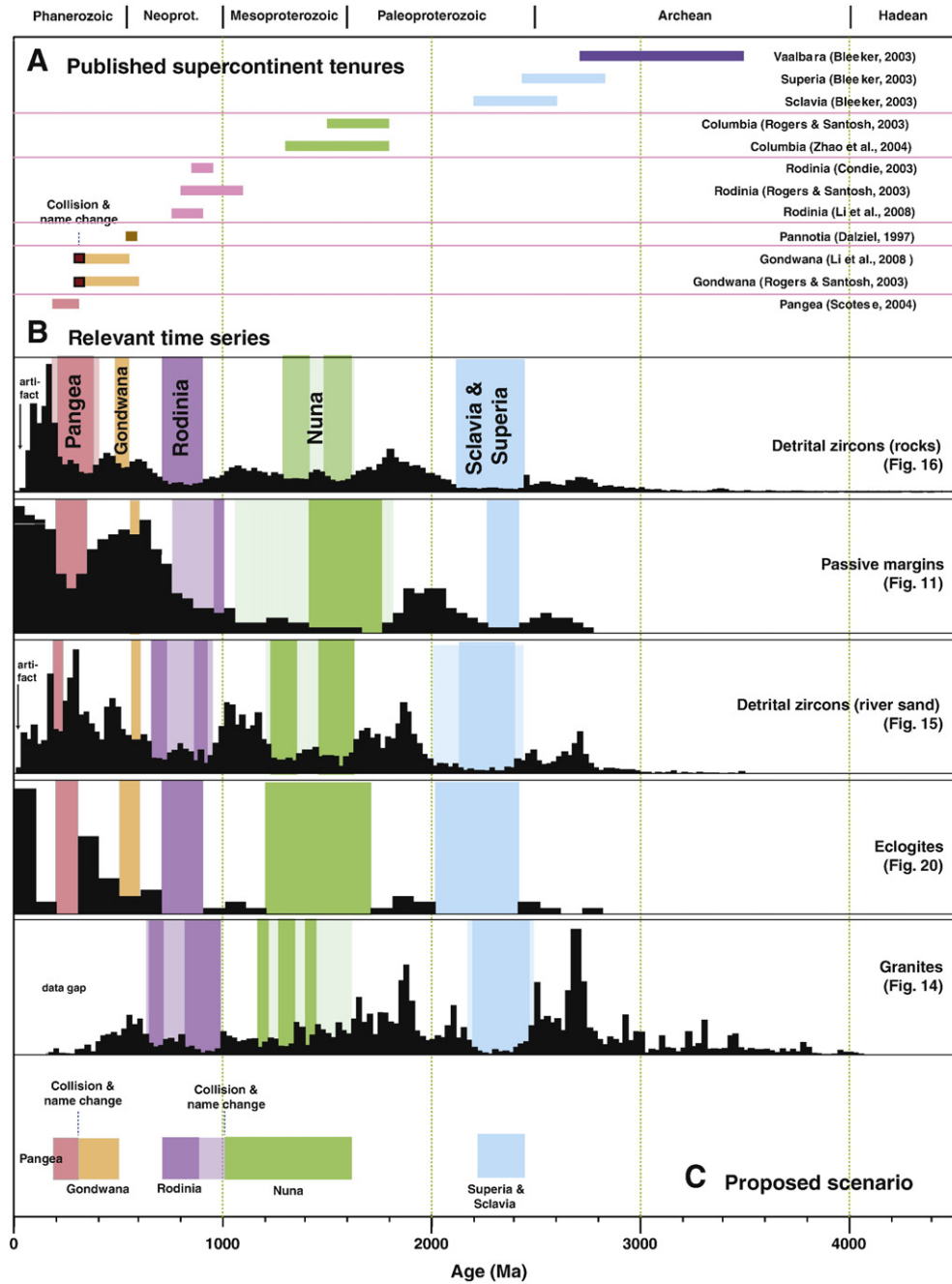


Fig. 46. (A) Published assessments of the tenures of various supercontinents according to the identified authors. (B) Age distributions (in black) of variables that have bear on the tenures of supercontinents, from sources cited in Figs. 11, 14, 15, 16, and 20. For each plot, the blue, green, lavender, orange, and pink swaths indicate tenures of supercontinents as inferred from minima in those data alone. Dimmer and brighter colors represent more and less inclusive interpretations, respectively. The colored swaths agree in general but differ in many details. (C) Proposed tenures of supercontinents based on the present study, combining information from Phanerozoic plate reconstructions, passive-margin age distributions, and zircon age distributions.

secular record shows probability maxima in granite abundance at 2700, 1893, and 569 Ma, as well as a number of subsidiary peaks.

This approach does have a number problems: (1) global data coverage is uneven, being thinnest in remote areas; (2) countless plutons have been lost from the geologic record, either buried beneath sedimentary cover, or utterly gone like the Hadean source plutons of the Jack Hills detrital zircons; (3) classification of some granites as “orogenic” or not can be equivocal; and (4) $^{40}\text{Ar}/^{39}\text{Ar}$ ages were not compiled, resulting in an undercount of Mesozoic and Cenozoic igneous rocks. The Phanerozoic part of the census is meager indeed, wrongly giving the impression that zircon production has declined to zero since the Jurassic. The compilation includes no modern volcanoes

and leaves out, or barely accounts for, enormous magmatic provinces such as the Okhotsk Chukotsk belt, the Patagonia batholith, and the Sierra batholith. Even knowing when to look for it, the tenure of Pangea cannot be discerned in this age distribution. Accordingly, there is direct no way to calibrate Fig. 14 against the only unequivocal part of the supercontinent cycle.

Detrital zircon data take care of some of the shortcomings of the granite data. Two general approaches have been used in global compilations of detrital zircons. Rino et al. (2008) and Campbell and Allen (2008) each dated thousands of detrital zircons from modern sands of major rivers, the idea being that these rivers collect a representative sampling of zircon from their drainages. Fig. 15 shows Campbell and

Allen's (2008) histogram based on 40 rivers. Maxima are seen at 2706, 1871, 1035, 447, 282, and 165 Ma and minima at 2565, 2247, 1576, 1294, 929, 671, 424, and 2233 Ma (Fig. 15). This compilation, and a similar one by Rino et al. (2008) (Fig. A21) share one shortcoming: the world's biggest rivers mainly traverse ancient cratons. Young orogenic belts are mostly drained by smaller rivers and there are no rivers of any size on many island arc volcanoes. Consequently, the paucity of detrital zircons younger than about 150 Ma is at least partly an artifact.

Detrital zircons from sandstones and metasediments provide another approach to global zircon distributions. The recent surge in the use of detrital zircon geochronology in studies of provenance and regional tectonics has already yielded at least a million individual zircon dates. Fig. 16 shows a new compilation of >26,000 zircon ages. Of the >350 sandstone and metasediment samples in this database, 21 are Archean, 69 are Proterozoic, and 122 are Cambrian through Triassic, and 140 are Jurassic or younger. Only this last group of samples has the potential to bear on zircon abundance during the Pangea supercontinent cycle. The overall age distribution shows maxima at 2729, 1824, 1793, 1435, 1047, 594, 432, 141, and 76 Ma and minima at 2374, 1565, 1371, 853, 529, and 367 Ma.

The fact that three independent zircon datasets (Figs. 14, 15, and 16) show comparable age distributions means that this cannot be an artifact of uneven sampling (Condie et al., 2009a). The possibility remains, however, that it is a different kind of artifact—one due to uneven preservation. Hawkesworth et al. (2010) took the latter position, suggesting that zircons generated during supercontinent-forming collisions are well situated to be preserved, whereas zircons along intraoceanic arcs are less so. This is an important problem. I submit that uneven preservation cannot readily account for the broad similarities between the abundances of passive margins and detrital zircons (cf. Figs. 11 and 16), or fluctuations in seawater $^{87}\text{Sr}/^{86}\text{Sr}$ (Figs. 17 and 18), as discussed in Section 4.4.

Adapting the arguments of Silver and Behn (2008), I postulate that the first order fluctuations in zircon abundance can be related to the supercontinent cycle as follows. (1) Most zircons are generated during plate convergence, either subduction or collision. (2) Supercontinent assembly involves subduction followed by continent–continent collision (Fig. 2). (3) The formation of a supercontinent extinguishes the convergent plate boundaries along which it formed. It follows that once a supercontinent has formed, global zircon production should decline sharply. The only way around this is if, upon the death of a collisional plate boundary and without delay, the equivalent amount of convergence begins to be taken up elsewhere on new or pre-existing subduction zones. Silver and Behn (2008) pointed out that subduction initiation has not accompanied the Himalayan collision, even though 50 million years have elapsed since collision started. (4) Hence, the tenure of a supercontinent should be marked by a dearth of zircons that lasts as long as the supercontinent itself. (5) Breakup should coincide with a rise in subduction-related magmatism (and by inference, an increase in zircon production), because new plate divergence in one place on Earth must be matched by plate convergence elsewhere.

If above reasoning is correct, an implication is that zircon abundance can potentially serve as a global plate speedometer. What is needed is a large suite of carefully chosen samples from various tectonic settings, from all parts of the world, and from each of the past 30 or more geons. As a first approximation from the less carefully selected datasets in Figs. 14–16, it would appear that at ca. 2300 Ma, global subduction flux (F_s of Silver and Behn, 2008) was 10–20% as fast as during the peaks of zircon abundance at ca. 1800 or 2700 Ma.

4.4. Isotopic composition of seawater strontium

The global $^{87}\text{Sr}/^{86}\text{Sr}$ ratio has increased through time owing to the inexorable decay of the world's initial allotment of ^{87}Rb to ^{87}Sr . Rubidium, meanwhile, has been concentrated in the continents, and continental rocks accordingly have elevated $^{87}\text{Sr}/^{86}\text{Sr}$ values. Sea

water $^{87}\text{Sr}/^{86}\text{Sr}$ is plotted for the Phanerozoic in Fig. 6 and for the entire span of Earth history in Fig. 17. These isotopic ratios were measured from over five thousand marine calcite samples/shells from the Phanerozoic and limestones from the Precambrian (Shields and Veizer, 2002). The lowest values of a given age are taken to most closely track the composition of seawater. The seawater curve represents the ever-shifting balance between sources of primitive mantle strontium (low $^{87}\text{Sr}/^{86}\text{Sr}$ that systematically rose through time), which mostly enters seawater via hydrothermal circulation at mid-ocean ridges, and evolved continental strontium (high but regionally variable $^{87}\text{Sr}/^{86}\text{Sr}$), which is carried to the sea by rivers and by fresh and saline groundwaters (Veizer and Mackenzie, 2003, and references therein). Because $^{87}\text{Sr}/^{86}\text{Sr}$ is a ratio, uneven preservation is less of a problem than for variables that require counting such as passive margin abundance.

In the Phanerozoic, the $^{87}\text{Sr}/^{86}\text{Sr}$ data show a sawtooth descent from ca. 500 to ca. 260 Ma, a double low at ca. 260 and ca. 160 Ma, and a long-term rise from ca. 160 Ma to the present. This first-order pattern broadly tracks the Pangea supercontinent cycle, with the shorter-term fluctuations corresponding, perhaps, to individual Wilson Cycles. The maxima are most likely the result of collisional orogenesis, which results in erosion of large volumes of high $^{87}\text{Sr}/^{86}\text{Sr}$ rock (Richter et al., 1992) and the death of a spreading center, eliminating an erstwhile source of low $^{87}\text{Sr}/^{86}\text{Sr}$.

For most of the Precambrian, age resolution is not as good, and the fine texture seen in the Phanerozoic $^{87}\text{Sr}/^{86}\text{Sr}$ seawater curve cannot yet be discerned (Veizer and Mackenzie, 2003) (Fig. 17). Nonetheless, first-order fluctuations are recorded. Fig. 18, which is derived from the same raw data, isolates the continental contribution to seawater $^{87}\text{Sr}/^{86}\text{Sr}$ by correcting for the mantle and carbonate weathering components (Shields, 2007). The seawater $^{87}\text{Sr}/^{86}\text{Sr}$ curve first deviated from the mantle evolution line at about 2800 Ma. A maximum in Fig. 18 at roughly 2000 to 1800 Ma coincides with the assembly of Nuna, and a minimum at roughly 1100 to 800 Ma overlaps with the nominal tenure of Rodinia. The six dashed sections of the curves in Figs. 17 and 18 were interpolated across times of sparse or nonexistent data. Judging from the Phanerozoic, low values of seawater $^{87}\text{Sr}/^{86}\text{Sr}$ would be expected at ca. 2300 Ma and ca. 850 Ma, and a high would be expected at ca. 1050 Ma. New data will be needed to test these predictions.

4.5. Deformation ages of greenstone belts

Greenstone belts are deformed accumulations of supracrustal rocks containing at least some volcanic component (Condie, 1994). The term is a catch-all and includes rocks inferred to have formed in ocean floor, intraoceanic arcs, continental arcs, forearc, intra-arc and back-arc basins, and oceanic plateau settings—especially in the Precambrian. Few Phanerozoic oceanic sequences have been categorized simply as greenstone belts. For both of these reasons, the age distribution of greenstone belts (Fig. A22, from Condie, 1994) is of uncertain significance. However, by combining rocks of many tectonic settings, deformation ages of greenstone belts (Fig. 19, from Condie, 1994) together provide a global record of convergent tectonism in the Precambrian. Orogenies involving greenstone belts were most abundant at ca. 2700, 1850, 1050, and 600 Ma; the Precambrian age distribution is broadly similar to that of granites and detrital zircons and a general connection with the supercontinent cycle is evident.

4.6. Eclogite and granulite facies metamorphism

The distribution of extreme metamorphic conditions through time suggests links with the supercontinent cycle (Brown, 2007, 2008). Exhumed eclogite facies metamorphic belts reached their peak abundance at 400–300 Ma, synchronous with the terminal collisions that formed Pangea; older peaks, based on fewer instances, are seen at ca. 2500–2400, 1900–1800, and 700–600 Ma (Fig. 20). Exhumed high

temperature (granulite facies) and ultra high temperature metamorphic belts reached their peak abundance at ca. 600–500 Ma with minor peaks at 2800–2500, 2100–1800, and 1100–1000 (Fig. 21). Given the paucity of exposed high temperature metamorphic rocks younger than ca. 500 Ma, the Pangea cycle is of no help in relating this style of metamorphism to supercontinents. In both plots, however, the Precambrian maxima broadly match those in the age distributions of granites and detrital zircons (Figs. 14–16) and broadly correlate with the supercontinent cycle (Brown, 2007). High pressure metamorphic rocks and metamorphic conditions are discussed in Section 6.4.

4.7. Carbonatites

The age distribution of carbonatites (Fig. 22, from Woolley and Kjarsgaard, 2008) is sufficiently similar to those of granites and detrital zircons that a general connection with the supercontinent cycle appears likely. Binned in 50 m.y. increments, peak abundances are at 50–0 and 150–100 Ma, and the most prominent minor peaks are at 250–200, 400–300, 600–500, 1050–1000, 1900–1850, 2100–2000, and 2700–2650 Ma. Carbonatites have not been reported from before ca. 2800, or between 2400 and 2150, 1550 and 1450, or 1300 and 1250 Ma. Carbonatites are widely interpreted as being related to extensional tectonic regimes, and specifically to continental breakup (e.g., Burke et al., 2003; Rukhlov and Bell, 2010). In this regard, aspects of the age distribution are problematic. The dominance of Triassic and younger carbonatites is probably exaggerated by attrition of older carbonatites, an effect discussed in Section 6.2. The minor peak at 250–200 Ma lies squarely during Pangea's tenure but the peak at 400–300 coincides with Pangea's assembly. The Precambrian maxima and minima are essentially the same as those in the orogenic granite or detrital zircon age distributions (Figs. 14–16). Except for the high at 2100–2000 Ma, the Precambrian maxima are times dominated by continental assembly, not breakup.

4.8. Large igneous provinces

Large Igneous Provinces (“LIPs”) are outpourings of mafic volcanic rocks and cogenetic intrusive rocks, commonly regarded as having formed above mantle plumes. Young LIPs include continental flood basalt provinces and oceanic plateaus. Ancient LIPs are recognized from flood basalts, layered mafic ultramafic intrusions, dike swarms, and, more controversially, komatiites (see Section 6.5). The distribution of LIPs through time is plotted in Fig. 23 from Prokoph et al. (2004), which was a minor update of the comprehensive synthesis by Ernst and Buchan (2001). The Phanerozoic is dominated by a broad peak at 200–0 Ma. This is likely magnified by the inclusion of the many LIPs in the present ocean basins; most of these will end up being subducted. Before 180 Ma, the LIP record is almost entirely continental and thus is not directly comparable to the younger record. The age distribution shows maxima at 2800–2700, 2200–2100, 1800–1700 Ma, and 1300–1200 Ma, and minima at 2400–2300, 1600–1500, 900–800, and 500–300 Ma. These four minima coincide with the tenures of supercontinents as deduced from the zircon and passive margin records.

5. Proposed supercontinent timetable

The tenures of supercontinents are shown from published literature in Fig. 46A. Fig. 46B shows the principal individual secular records that bear on the timing of supercontinents. A proposed supercontinent timetable is shown in Fig. 46C, modified from Bradley (2008) subject to the age constraints provided by the time trends shown. The present study does not bear on the details of particular supercontinent reconstructions.

5.1. Vaalbara, Superia, and Sclavia (Bleeker, 2003) or Kenorland (Williams et al., 1991)

The earliest continental assemblies are quite conjectural. Williams et al. (1991) postulated a single Neoproterozoic supercontinent, Kenorland, that was assembled by ca. 2500 Ma. Later, Bleeker (2003) identified three smaller continental groupings based on common themes among the world's 35 known Archean crustal blocks: Vaalbara, Superia, and Sclavia. Vaalbara, the oldest, includes the Kaapvaal and Pilbara cratons and was proposed by Bleeker (2003) to have existed from ca. 3470 to ca. 2700 Ma. Superia includes Canada's Superior craton plus other continents that rifted from it during the Paleoproterozoic (e.g., Karelia, Hearn); Bleeker (2003) gave its age range as ca. 2700 to 2450 Ma. Sclavia includes Canada's Slave craton and various other cratons that rifted away from it during the Paleoproterozoic (e.g., Dharwar, Zimbabwe); Bleeker (2003) suggested an age range from ca. 2600 to 2200 Ma. Based on passive margin ages, Bradley (2008) suggested minor modifications to Bleeker's timing: Vaalbara from ca. 3470 to ca. 2685 Ma, Superia from ca. 2700 to ca. 2300 Ma, and Sclavia from ca. 2600 to ca. 2090 Ma.

Bleeker (2003) coined the term *supercraton* for these continental groupings because none of the three were considered large enough to meet the “all or nearly all” definition of supercontinent. A key question is whether the assembly, tenure, and disassembly of these three continental masses would have caused global plate reorganizations. In each case the answer is yes. The breakup of Superia, for example, involved the initiation of at least four new divergent plate boundaries surrounding the Superior craton, totaling thousands of kilometers in length. In order to accommodate these ridges, suitably oriented subduction zones must either have formed or, if already in existence, must have begun consuming seafloor at a faster rate.

The abundances of orogenic granites and detrital zircons show huge fluctuations during the span between the putative assembly of Vaalbara and the breakup of Sclavia, ca. 3470 to 2090 Ma. The dearth of granites between 2400 and 2200 Ma and of detrital zircons between 2400 and 2300 Ma coincides the simultaneous tenures of Superia and Sclavia. (An equivalent low during the putative tenure of Vaalbara is not in evidence.) The remarkable maxima in granite and detrital zircon abundances at ca. 2700 to 2600 Ma coincide with the proposed assembly times of both Superia and Sclavia. If, alternatively, Vaalbara, Superia, and Sclavia occupied far removed portions of a single Kenorland supercontinent (Bleeker, 2003, his Fig. 5a), the zircon record (Figs. 14, 15, and 16) would suggest staged assembly from ca. 2750 to 2450 Ma followed by a dead time of supercontinent tenure lasting to ca. 2200 Ma (cf. Condie et al., 2009b).

5.2. Nuna

Paleoproterozoic breakup of Sclavia and Superia (or alternatively, of Kenorland) led to a time of dispersed continents, as suggested by a peak in the abundance of passive margins between ca. 2050 and ca. 1900 Ma (Fig. 11). Each margin was eventually involved in a collision, creating a new continental grouping and leaving no passive margins at all from ca. 1740 to ca. 1600 Ma. This late Paleoproterozoic continental grouping was called Nuna by Hoffman (1997) and Columbia by Rogers and Santosh (2002). The case that all the world's continents were gathered into a *single* grouping is not compelling but under my definition of supercontinent, Nuna would qualify regardless. Various proposed configurations are quite different (cf. Hoffman, 1997, Rogers and Santosh, 2003, and Zhao et al. 2002). Hoffman (1997) suggested that Laurentia, Greenland, and Baltica had come together by 1800 Ma. According to Rogers and Santosh (2003), Columbia came together at ca. 1800 Ma and broke apart ca. 1500 Ma. According to Zhao et al. (2002), it came together (but in a very different configuration) by a series of collisions from 2100 to 1800 Ma,

grew by subduction accretion until ca. 1300 Ma, and then broke up, to reform soon thereafter as Rodinia.

The granite and detrital zircon records (Figs. 14–16) are consistent with the late Paleoproterozoic assembly of a supercontinent. The detrital zircon maximum at 1824 Ma (Fig. 16) can be attributed to Nuna forming collisions, and the ensuing decline in zircon abundance to a minimum at 1565 Ma can be attributed to the death of a number of convergent plate boundaries when Nuna came together.

The passive margin record is also consistent with the late Paleoproterozoic assembly of a supercontinent. An abundance of passive margins between ca. 1850 and 2050 Ma was followed by a precipitous drop between ca. 1850 and 1750 (Fig. 11). This would correspond to the assembly of Nuna and is consistent with the various published interpretations cited above. On the other hand, the passive margin record (Bradley, 2008) provides no independent confirmation of the proposal that subsequently, during the Mesoproterozoic, a supercontinent broke up and then reformed into Rodinia (cf. Rogers and Santosh, 2003 and Zhao et al. 2002). The Mesoproterozoic was a time of few passive margins; at no time between 1750 and 1000 Ma was there a sudden increase in their abundance like that seen in the Phanerozoic upon the breakup of Pangea. This suggests that Nuna remained intact until at least 1000 Ma.

Relative quiescence during the tenure of a Mesoproterozoic supercontinent provides an explanation for the “Boring Billion” of Holland (2006). Secular records that show pronounced minima during the ca. 1600–1000 Ma interval include passive margins (Fig. 11), detrital zircons (Figs. 15 and 16), seawater $^{87}\text{Sr}/^{86}\text{Sr}$ (Fig. 18), greenstone belt collisions (Fig. 19), eclogites (Fig. 20), granulites (Fig. 21), carbonatites (Fig. 22), and orogenic gold (Fig. 37).

5.3. Rodinia

The next supercontinent, Rodinia, is generally regarded as having been assembled near the end of the Mesoproterozoic and disassembled in stages during the Neoproterozoic. Reconstructions of Rodinia are notable for their lack of agreement. Differing interpretations of the position of West Africa were listed in Section 1; southwestern Laurentia is equally controversial, being variously positioned next to East Antarctica (Moore, 1991), Australia (Karlstrom et al., 2001), Siberia (Sears and Price, 2003), South China (Li et al., 2008) or West Africa (Evans, 2009). Most reconstructions are variations on a theme in which two halves of Rodinia came together during the Grenville orogeny. In the very different model recently suggested by (Evans (2009), the Grenville orogen was not the result of a terminal, supercontinent forming collision, but instead was an Andean type orogen that faced a Pacific type ocean, external to Rodinia. A common element in all these reconstructions is the yet unproven assumption that most or all the world's continents were part of a *single* supercontinent. Whether they all were or not, the key point is that at least *many* of the continents were together. This is evident from the initiation of new rifted margins on all sides of Laurentia at about the time of the Neoproterozoic Cambrian boundary (e.g., Hoffman, 1991).

Published assessments of Rodinia's dates are in general agreement. Condie (2003a) suggested that it was assembled between 1300 and 950 Ma, that it lasted from 950 to 850 Ma, and was disassembled from 850 to 600 Ma. Similarly, Li et al. (2008) suggested that Rodinia was assembled between 1300 and 900 Ma, was at its largest from 900 to 750 Ma, and was disassembled in stages from about 790 to 550 Ma (Li et al., 2008, animation).

I suggest a slightly different scenario and timetable based on the passive margin and zircon records. Abundances of detrital zircons show a major peak at 1044 Ma and a subsequent low centered at 900–850 Ma (Fig. 16), consistent with the assembly of a Rodinia supercontinent during Grenville age collisions. Comparable age patterns are evident in the age distributions of greenstone belt collisions, eclogite and granulite facies metamorphism, and carbona-

tites (Figs. 19–22). Knowing to look for it, this age pattern can be dimly made out in the orogenic granite plot (Fig. 14). On the other hand, passive margin and detrital zircon abundances, which were in synch during the assembly and early tenure of Nuna, fall out of phase during the putative assembly of Rodinia. Only two passive margins are known from ca. 1200 to 1050 Ma, when their number started gradually rise, eventually reaching 24 by 600 Ma. Considering the detrital zircon and passive margin records together, it would appear that orogenies during the assembly of Rodinia did not involve passive margins (Bradley, 2008). During several hundred million years leading up to the Grenville orogeny, eastern Laurentia was the site of a long lived convergent margin (Hoffman, 1991; Whitmeyer and Karlstrom, 2007); when the last seafloor was consumed along this orogen, the global abundance of passive margins is not known to have changed. I submit that the early Neoproterozoic minimum in detrital zircon abundance at ca. 1000 to 850 Ma best represents Rodinia's tenure. It appears, though, that one part of Rodinia was already being disassembled (i.e., along Baltica's Uralian margin; Bradley, 2008) while elsewhere, along the Grenville orogen, Rodinia's assembly was still underway. The Rodinia supercontinent cycle departed from the ideal.

5.4. Gondwana

Whether or not the next continental assemblage Gondwana qualifies as a supercontinent depends on the definition, as discussed in Section 2. Only if one adopts an inclusive definition, as I now do, does Gondwana qualify. Gondwana consisted of the cratons now in South America, Antarctica, Africa, Arabia, India, and Australia, as well as microcontinents in the Appalachian and Paleotethyan realms. Its fit is well constrained because the now dispersed pieces can be brought together by closing the modern South Atlantic, Indian, and Southern Oceans; the Gondwana fit is essentially the southern half of the Pangea fit.

In the geologically and paleomagnetically based animation of Li et al. (2008), collisional assembly of Gondwana is shown spanning the interval 690 to 530 Ma. This timing is consistent with the peak abundance of passive margin end dates at 650–550 Ma (Fig. 13), with the peak abundance of detrital zircons at 600–550 Ma (Fig. 16), and with the peak abundance of orogenic granites at 588 Ma (Fig. 14). These secular trends conform to the patterns seen for Pangea. A key point is that the assembly of Gondwana and disassembly of Rodinia overlapped in time. The final breakup of Rodinia, marked by the rift drift transition along the Ouachita passive margin, is dated at about 520 Ma (Bradley, 2008, and references therein).

Gondwana remained largely intact until colliding with Laurentia at about 300 Ma. Then it underwent a name change, becoming part of Pangea, which broke up starting ca. 180 Ma. Thus, the tenure of Gondwana can be set at ca. 550 to ca. 180 Ma.

6. Supercontinent cycles and other secular variation

Using the revised timetable (Fig. 46C) as a baseline, I next discuss secular trends that bear on the evolving context of the succession of supercontinents and on the properties of particular cycles. The differences between cycles can be attributed to factors such as the vagaries of plate geometry, long term decline of Earth's radiogenic heat production, long term increase in viscosity of the residual mantle, emergence of life as a major geochemical agent, and oxygenation of the oceans and atmosphere. Many Earth processes are cyclic, for different reasons and on different timetables, and interactions among different cycles have led to remarkable secular changes.

6.1. Global heat production and rates of plate tectonics

The heat generated by the decay of ^{238}U , ^{235}U , ^{232}Th , and ^{40}K has exponentially declined through Earth history (Fig. 24, from Pollack, 1997). The various curves correspond to different mixes of radioactive

fuel, with the “crustal” curve corresponding quite closely to [Allegre et al. \(2001\)](#) assessment of the bulk composition of the Earth. Regardless of the fuel mix, all published variations of this curve have the same basic form, showing an exponential decline in radiogenic heat production since the beginning.

Mantle potential temperature, as inferred from the geochemistry of non arc basalts, shows a cooling trend over the latter half of Earth history ([Fig. 25](#); from [Herzberg et al., 2010](#)). Temperatures were as high as 1500–1600 °C at ca. 3000–2500 Ma, and have declined since. Each successive supercontinent cycle thus played out on a cooler planet.

Early Earth's extra heat is behind the widely held belief in the geodynamics community that Precambrian global spreading rates were higher, and that the early Earth was occupied by smaller and (or) faster plates (e.g., [Burke et al., 1976](#); [Hargraves, 1986](#); [Pollack, 1997](#)). Alternatively, based largely on paleomagnetic evidence, [Kröner and Lauer \(1992\)](#) suggested that Archean rates of plate motion were comparable to modern rates. More recently, [Korenaga's \(2006\)](#) modeling of mantle evolution suggested an overall *increase* in global spreading rate through the first 95% of Earth history; it has only declined since about 300 Ma ([Fig. 26](#)). The rationale is that higher degrees of partial melting of the hotter mantle beneath ridges would have produced thicker oceanic crust ([Fig. A30](#), from [Moore, 2002](#)) and a substantially more viscous residual mantle, resulting in slower global spreading rates than today ([Korenaga, 2006](#)). As supporting geologic evidence, [Korenaga \(2006\)](#) cited an apparent decrease in the period between supercontinents over time. A new line of supporting evidence – and one that does not hinge on the subjective definition of what is or isn't a supercontinent – is provided by the longer lifespans of individual passive margins in the Proterozoic ([Fig. 27](#); see [Section 6.2](#)) ([Bradley, 2008](#)).

Shorter term fluctuations in global spreading rates are another matter. The Late Cretaceous, in particular, has been widely regarded as a time of faster spreading rates ([Hays and Pitman, 1973](#)), although a recent reappraisal by [Rowley \(2002\)](#) found no supporting evidence in the slim magnetic anomaly record. Slower global spreading rates are to be expected during times of supercontinent tenure ([Silver and Behn, 2008](#)), but there is no seafloor record with which to directly test this idea.

Additional secular trends bearing on the physics and chemistry of the mantle are shown in [Figures A30, A31, A33, A36, A38, A40, and A41](#).

6.2. Oceanic crust and passive margin proxies

The age distribution of oceanic crust is akin to that of a human population, with spreading like birth and subduction like death ([Veizer and Jansen, 1979, 1985](#); [Veizer et al., 1989](#); [Veizer and Mackenzie, 2003](#)). The proximal cause of this age pattern ([Fig. 8](#); from [Sclater et al., 1980](#)) is attrition: only survivors are counted. Based only on the current situation, oceanic crust would appear to have an oblivion age of about 180 Ma, a half life of about 60 m.y., and a recycling rate of about 3.5 km²/yr ([Veizer and Mackenzie, 2003](#)). These particular values, however, are contingent on our current place in the supercontinent cycle. Thirty million years from now, the Atlantic will have widened, the apparent half life of the world's oceanic crust will be longer, and the apparent recycling rate slower.

For the deeper past we can glean anecdotal information from the passive margin compilation described in [Section 4.2](#). The lifespan of a passive margin ([Fig. 27](#)), namely its start date minus its end date ([Bradley, 2008](#)), is dictated by the rates of plate motion during opening and closing phases of the ocean basin. These dates can be recast to track the age of the oldest Atlantic type seafloor through time ([Fig. 28](#); see [Supplementary data](#) for explanation); this works because of the equivalence between the lifespan of a passive margin and the age (at time of collision) of the oldest seafloor that bordered it.

Atlantic type oceanic crust has generally lasted longer than it does on Earth at present³. Based on an equivocal stratigraphic record from Siberia, the oldest seafloor evidently endured for nearly 600 m.y. before finally being subducted at about 1000 Ma ([Bradley, 2008](#)). In the sawtooth curve in [Fig. 28](#), the longest lived margin at a given time ages along a line with slope of –1 until collision, when a different margin takes over as oldest. Steady increases from 2444 to 2130, 1600 to 1010, 849 to 558, and (less strikingly) 299–160 Ma correspond to tenures of Sclavia and Superia (S S), Nuna (N), Rodinia (R), and Pangea (P).

6.3. Obducted ophiolites

Obducted ophiolites fragments of ancient oceanic lithosphere caught up in orogenic belts have an uneven age distribution. [Figs. 9 and 29](#) (from [Moore, 2002](#) and [Dilek, 2003](#)) show maxima at ca. 800–750, 500–450, 160–150, and 100–90 Ma. The Ordovician peak largely reflects Appalachian forearc ophiolites ([Cawood and Suhr, 1992](#)) that were obducted during the earliest phases of Pangea's assembly. The two Mesozoic peaks, which mostly correspond to ophiolites in the Tethyan realm, are broadly synchronous with disassembly of Pangea. The scarcity of ophiolites younger than 70 Ma rules out attrition as the main reason behind the age distribution. Whereas a single explanation in terms of some aspect of the supercontinent cycle is elusive, it is clear that the vast majority of ophiolites formed and were obducted during some part of the Pangea cycle.

6.4. High pressure, low temperature metamorphic rocks

High pressure, low temperature metamorphic rocks, classic indicators of plate convergence, form during subduction of both oceanic and continental crust. [Fig. 30](#) shows the distribution of blueschists and ultra high pressure metamorphic rocks through time ([Brown, 2007](#)). The oldest blueschists date from assembly of Gondwana (ca. 680 Ma blueschists from Brazil; [Parkinson et al., 2001](#)). In the Phanerozoic ([Fig. A2](#)), blueschists and ultra high pressure metamorphic rocks are relatively abundant from ca. 400 to 300 during assembly of Pangea, and from ca. 100–50 Ma during disassembly of Pangea. They are relatively scarce from 300 to 150 Ma, during Pangea's tenure ([Fig. A2](#)). Thus, their age distribution is broadly consistent with the Pangea supercontinent cycle.

The greatest metamorphic pressures are seen in Phanerozoic rocks ([Fig. 31](#), from [Brown, 2008](#)) whereas the steepest inferred geothermal gradients, based on sparse data, are seen in Paleoproterozoic rocks ([Fig. 32](#), from [Brown, 2008](#)). The most straightforward interpretation is that blueschists and related rocks are absent from the record before the Neoproterozoic because P–T conditions in subduction zones were different.

6.5. Mantle derived igneous rocks

Secular cooling of the mantle ([Section 6.1](#)) is broadly consistent with the age distribution of the ultramafic volcanic rock, komatiite. A probability density plot ([Fig. 33](#); constructed from [Table 1](#) of [Isley and Abbott, 1999](#)) shows peak abundances of komatiites at ca. 3400 and 2750 Ma, and a single occurrence in the Cretaceous. [Figure A40](#) shows the abundance of komatiite relative to other volcanic rocks in the greenstone belts in which they occur (from [Condie and O'Neill, 2010](#)), after a similar plot by [de Wit and Ashwal, 1997](#)); the ratio confirms that the prominent peak at ca. 2750 Ma in [Fig. 33](#) is not merely an artifact of preservation. Potential temperatures for komatiites are substantially higher than for modern basalts, roughly 1600–1800 °C ([Herzberg et al., 2010](#)) ([Fig. 25](#)). Komatiites have been most widely interpreted as the products of mantle plumes ([Ernst and Buchan,](#)

³ This analysis does not bear on the longevity of Pacific-type oceanic crust through time, and thus tells only part of the story.

2001; Isley and Abbott, 2002), although a subduction origin has also been advocated (Grove and Parman, 2004). Regardless, the early abundance of komatiites implies that the mantle was hotter than today and that by ca. 1700 it had cooled sufficiently that komatiites became exceedingly rare. This explains their occurrence in orogens related to assembly of Vaalbara, Superia, Sclavia, and Nuna and their absence in orogens formed during assembly of Rodinia, Gondwana, or Pangea.

The neodymium isotopic system, based on the decay of ^{147}Sm to ^{143}Nd , is a good tracer of both crustal and mantle evolution because Sm and Nd fractionate during partial melting at mantle depths.⁴ The neodymium isotopic composition of the depleted mantle is thus more radiogenic (positive ϵ_{Nd}) than that of the continental crust (negative ϵ_{Nd}). Fig. 34 (from Bennett, 2003) tracks ϵ_{Nd} of proxies for the depleted mantle over time, specifically modern MORBs, Phanerozoic ophiolites, and Precambrian juvenile granitoids. The data show a clear secular increase in ϵ_{Nd} of the depleted mantle, toward ever more radiogenic values. The general clustering of analyses from around 2700–2500, 2100–1800, and 600–500 Ma is probably a reflection of the relative abundance of rocks of these ages. Each supercontinent formed in the context of ever more depleted mantle. The data are yet too sparse to show whether the overall increase was steady, or punctuated by the supercontinent cycle.

The subcontinental lithospheric mantle evolved as the succession of supercontinents came and went. Mantle xenoliths and xenocrysts from beneath crustal provinces of various ages show systematic variations through time in density (Fig. 35), mineralogy (Fig. A30), and chemistry (Fig. A31) (Poudjom Djomani et al., 2001; Griffin et al., 2003; Griffin et al., 2009). Archean cratons have deeper, more buoyant, more depleted keels than Proterozoic or Phanerozoic continents. The age resolution of these findings is still too coarse to reveal any secular variations on the time scale of individual supercontinent cycles.

6.6. Massif type anorthosites

Massif type anorthosites (plutons having >90% plagioclase) have an unusual age distribution (Fig. 36) featuring a broad high from about 2000 to 1000 Ma, roughly the time of Holland's (2006) "Boring Billion". Not unexpectedly, a similar age distribution is shown by anorthosite-hosted titanium ores (Meyer, 1988; not shown). Massif type anorthosites first appeared in abundance during the assembly of Nuna and virtually disappeared after the assembly of Rodinia. The population is dominated by anorthosites from Laurentia and Baltica; the tectonic setting of emplacement appears to have been along a long-lived convergent margin (Ashwal, 1993). Hoffman (1989) suggested that the Laurentian anorthosites formed at a time of greater global heat production when Nuna sat almost immobile with respect to the mantle, a process that no longer can occur because of secular cooling.

6.7. Orogenic gold deposits

Orogenic gold deposits are products of plate convergence, being formed at mid-crustal levels during regional prograde metamorphism (Goldfarb et al., 2001). Peak abundances are seen at 2700–2600 and 200–100 Ma (Fig. 37). Few orogenic gold deposits would be expected at times of tectonic quiescence, during the tenures of supercontinents. Consistent with this prediction, since the Neoproterozoic, there are two major intervals when orogenic gold deposits are unknown: ca. 2500–2200 and ca. 1700–800 Ma. The older interval corresponds to the tenures of Sclavia and Superia (or of Kenorland); the younger interval corresponds to the combined tenures of Nuna and Rodinia. Orogenic gold deposits, however, are not particularly sparse during the tenures

of Gondwana or Pangea. The overall age distribution is therefore somewhat problematic.

6.8. Sedimentary rocks

Several compilations have shown that the global abundance of sedimentary rock decreases back through time. In a detailed plot of just the Phanerozoic (Fig. 10) (Veizer and Mackenzie, 2003, who attributed the plot to W.W. Hay), sedimentary rocks are subdivided into three depositional settings: epicontinental, passive margin, and ocean basin. The abundance of geologically young passive margin and ocean basin strata can be attributed to three effects: (1) attrition—the geologic destruction of these tectonic settings over time; (2) rules of the census, which discounted older oceanic or passive margin strata after they have been involved in orogeny; and (3) our current place about 180 m.y. into a supercontinent cycle.

Unfortunately, there is no comparable plot of sedimentary rock volume through the span of Earth history. The best available appears to be compilation of Ronov et al. (1991) (Fig. 38), which stopped well short, leaving out the Paleoproterozoic and Archean. This shows an overall decline back through time: younger strata are more abundant because older strata have been eroded away, subducted, or so tectonized that they are no longer counted as sedimentary rocks. Fluctuations that might correlate with older supercontinent cycles cannot be detected in this time-averaged dataset.

6.9. Sedimentary recycling

Veizer and Mackenzie (2003, and older references therein) estimated that the Earth's sedimentary mass is ~90% recycled from older sedimentary rock. The time scale of recycling is revealed by the neodymium isotopic composition of shales and sandstones (Fig. 39, from Vervoort et al., 1999), and by detrital zircons (Fig. 40). The x-axis in both plots is the depositional age. In Fig. 39, the y-axis is the crustal residence age, i.e. the time since the continental crust from which the sediments were derived originally separated from the mantle. In Fig. 40, a new plot, the y-axis is the igneous age of detrital zircons, typically 60 to 100 ages per sandstone sample. Both plots show that, relative to the time of deposition, sedimentary grains are older now than in the past. Thus, a sandstone deposited during the assembly of Nuna consisted of then newer clastic material than a sediment deposited during the assembly of Pangea. This makes it harder and harder to create so-called "juvenile crust" (cf. Fig. A27) during each successive supercontinent cycle.

6.10. Oxygenation of the atmosphere and oceans

Secular trends identify three tipping points in the oxygenation history of the exosphere, at ca. 2500, 1850, and 580 Ma. The existence of a "Great Oxidation Event" (or GOE) near the Archean-Proterozoic boundary has long been suspected and is now well documented by means of sulfur isotopes (e.g., Farquhar et al., 2010). Fig. 41 shows $\Delta^{33}\text{S}$ in a variety of sulfide and sulfate minerals is plotted as a function of time, from a compilation by Domagal Goldman et al. (2008). $\Delta^{33}\text{S}$ is a measure of mass-independent fractionation of sulfur isotopes. An abrupt, dramatic transition occurred from a range of both negative and positive values before ca. 2500 Ma, to near zero since then. The isotopes of sulfur fractionate independently of mass when solar UV radiation strikes sulfur-bearing dust in the atmosphere. Ozone in the stratosphere blocks solar UV radiation so its presence (and by extension, the presence of O_2 in the troposphere below) can be inferred starting at ca. 2500 Ma.

The age distribution of Superior-type banded iron formations (BIFs) reveals another transition at ca. 1850 Ma. BIFs were widely deposited between about 3000 Ma and about 1850 Ma, vanished from the record for about more than a billion years, made a brief resurgence

⁴ The hafnium isotopic system, based on the decay of ^{176}Lu to ^{176}Hf , is comparable to the neodymium system (Fig. A33).

associated with Neoproterozoic glaciations, and vanished again (Bekker et al., 2010) (Fig. 42). Superior type BIFs accumulated in platformal to outer ramp settings and many, at least, are associated with the terminal collisions of long lived passive margins (Hoffman, 1987). Precipitation of magnetite (the principal iron mineral in BIFs) from seawater requires reducing conditions and low concentrations of sulfur (Huston and Logan, 2004). Evidently, such conditions did not pertain before ca. 3200 Ma or after about 1850 Ma. The apparently simultaneous global demise of BIFs at 1850 Ma coincides with the Sudbury impact event in Canada (Slack and Cannon, 2008).

The concentration of molybdenum in marine black shales suggests a third transition at ca. 580 Ma. Before that time, Mo concentrations ranged from a few to about 70 ppm; after 580 Ma, Mo concentrations jumped by an order of magnitude (Fig. 43; Scott et al., 2008). Scott et al. (2008) inferred that this transition dates the oxidation of the deep ocean and advent of the redox and nutrient cycles that pertain today.

Campbell and Allen (2008) have suggested that these transitions in the behaviors of sulfur, iron, and molybdenum were the result of supercontinent assembly. In this scenario, orogeny during supercontinent assembly supplies nutrients such as phosphorus and iron to the oceans in greater than normal amounts. This increases photosynthesis and oxygen production while also promoting burial of organic carbon.

6.11. Glaciation

Glacial intervals in Earth history took place during the assembly, tenure, and collision stages of various supercontinent cycles (Fig. 44). The Pleistocene ice sheets spread across the widely dispersed fragments of Pangea, long after its breakup. In contrast, the Paleozoic ice sheets of the southern hemisphere existed during times of supercontinent tenure: in the Pennsylvanian to Permian on Pangea, and in the Ordovician and Devonian on Gondwana. The regional Gaskiers glaciation at ca. 580 Ma took place during the overlapping time of Rodinia's breakup and Gondwana's assembly. This is also the case for the global Marinoan and Sturtian glaciations at ca. 635 and ca. 700 Ma. The Paleoproterozoic (ca. 2300–2200 Ma) Gowganda global glaciation correlates in general with the tenures of Sclavia and Superia. In a review of tectonic settings of glaciogenic rocks, Eyles (2008) found a preponderance that he interpreted as rift related.

6.12. Sea level

Some first order sea level changes can be correlated with the Pangea supercontinent cycle. Sea level as recorded by the proportion of platform flooding was generally high in the early and middle Paleozoic, low in the late Paleozoic to early Mesozoic, high during the Cretaceous, and relatively low today (Fig. 7, from Hallam, 1992). The broad low closely matches the tenure of Pangea as indicated by the area of the largest continent (Fig. 3) (Worsley et al., 1984, 1986). This correlation can be explained by a model proposed by Heller and Angevine (1985) that relates sea level change to ridge volume and to the supercontinent cycle. Continental breakup is followed by growth of an Atlantic type ocean at the expense of a Pacific type ocean, i.e., one that is bounded by subduction zones. At first, the new Atlantic type seafloor is younger than the average seafloor that is necessarily subducted elsewhere, so sea level rises. Later, the growing Atlantic type ocean becomes older than the average subducting seafloor, so sea level falls. Thus a lag is built into the process, such that the highstand follows initial opening by 70 to 120 m.y. (Heller and Angevine, 1985). Some of the finer texture of the Phanerozoic sea level curve may be due to the Heller and Angevine (1985) mechanism applied to individual ocean basins and individual Wilson cycles, each operating on slightly different timetables. Low sea level at the start of Pangea's tenure can be linked to the requisite death or slowing of mid ocean ridges when convergence ceased across the Central Asian, Uralian,

Appalachian, and Ouachita orogens. Similarly, the preceding major lowstand, at ca. 550 Ma (Fig. 7), correlates with the start of Gondwana's tenure (Condie, 2005).

The supercontinent cycle is not the only driver of sea level fluctuations. Others include glaciation (a contributor to the present day low) and the distribution of continents and ocean basins over geoid highs and lows. Proterozoic sea level fluctuations are still too poorly resolved to bear definitively on older supercontinent cycles.

6.13. Mississippi Valley type lead zinc deposits

Mississippi Valley type (MVT) lead zinc deposits are epigenetic lead zinc ores hosted in carbonate rocks (e.g. Leach et al., 2010). Their distribution through Earth history, as measured by amount of contained metals (Fig. 45) is dominated by Phanerozoic deposits and particularly by ones associated with the tenure of Pangea. Most MVT deposits are in passive margin platform sequences now located in fold thrust belts or orogenic forelands (Bradley and Leach, 2003). In the type area in the south central United States, MVT host carbonates were laid down along a Cambrian to Mississippian passive margin that originated during the last fragmentation of Rodinia. The margin was inundated by synorogenic clastics during the Ouachita orogeny, one of the last of the Pangea forming collisions, in the Pennsylvanian. The deposits themselves were formed in the orogenic foreland from a continent scale hydrothermal system that recharged in the orogen. Thus the host rocks are from the dispersal phase of one supercontinent cycle and the mineralizing event was part of the assembly phase of a second supercontinent cycle. As is the case for many types of ore deposits, MVT formation requires the confluence of other contributing factors as well. Specifically: (1) MVT deposits form from brines in the arid latitudinal belts at ca. 15–30°N and S (Leach et al., 2010 this is a nearly untapped exploration criterion); and (2) mineralizing brines must contain free oxygen, ruling out the existence of this type of deposit in the Archean.

6.14. Other secular trends

The plots in Figs. 3–45 bear on the supercontinent timetable, the evolving context of the succession of supercontinents, the properties of particular cycles, and long term background trends. Figures A1–A86 in the Supplementary data section show additional secular trends that were compiled for this study. They pertain to the continental crust, the mantle, granitoid chemistry, seawater chemistry, sedimentary chemistry, sedimentary rock types, the fossil record, ore deposits, and extraterrestrial variables. The number of recently published secular trends of global scope attests to the growth of this approach to Earth history.

7. Summary

Two complementary approaches to Earth history plate reconstructions and analysis of secular trends have been brought together in this assessment of the supercontinent cycle. A global plate reconstruction for a particular time provides a unified rationale for the origins of, interrelations between, and geographic distribution of the rocks of that age. In general, this approach gets harder and less certain back through time. A few intervals in the Precambrian, however, are more tractable: the supercontinent intervals. But each Precambrian supercontinent is subject to debate as to timing of assembly and breakup, configuration of the pieces, relative size, and even whether or not the term "supercontinent" should be applied.

The supercontinent cycle appears to be manifested in a number of secular trends. It is well suited to study by analysis of multiple trends because plate reorganizations, which necessarily take place when ocean basins start to open and when they finish closing (Silver and Behn, 2008), influence many parts of the Earth system. For present

purposes, the most informative trends are those that in some way track the assembly, tenure, and disassembly of Pangea. The tenure of Pangea was a time of few passive margins and a relative low in zircon production. Followed deeper into the past, these two variables together suggest that the tenures of putative Precambrian supercontinents coincided with zircon *minima* at ca. 2450–2225 (Superia and Sclavia, or Kenorland), ca. 1625–1000 (Nuna), and ca. 875–725 Ma (Rodinia). Other secular trends that show this same pulse include the abundances of granulites, eclogites, carbonatites, volcanogenic massive sulfides, and greenstone belt collisions.

The supercontinent cycle has been characterized as periodic (e.g. [Korenaga, 2006](#)). Indeed this is the obvious inference from older compilations such as [Condie's \(1997\)](#) plot of orogenic granites (Fig. A21), which shows three remarkable peaks in abundance at 2700–2600, 1900–1800, and 1100–1000 Ma. The case for true periodicity is not so compelling if one judges from more recent compilations of zircon abundances (Figs. 14, 15, and 16), which show a number of minor maxima and minima in addition to the main ones. How these lesser fluctuations relate to supercontinent assembly, tenure, and disassembly ties into whether or not a relatively small grouping of continents, like Gondwana, counts as a supercontinent. This is not merely a question of semantics; it underscores the need for a quantitative measure of “supercontinentality.”

Each supercontinent cycle was unique for multiple reasons. On Earth today we can see how intricate the shape and layout of the continents can be, and how complicated the mosaic of boundaries between plates, large and small. There is no reason to expect that things were ever much simpler during earlier times when continents were dispersed. Each supercontinent cycle was also unique because of its time in Earth history. The successive supercontinent cycles played out against inexorable long term changes related to Earth's declining radiogenic heat production. As the mantle cooled, the degree of partial melting beneath ridges decreased, and the viscosity of the residual mantle accordingly decreased. Taking this into account, [Korenaga's \(2006\)](#) modeling results suggest that through the Proterozoic, plate motions sped up, and that through the Phanerozoic, they slowed down. Once common rock types went virtually extinct: banded iron formation, komatiite, and massif type anorthosite. Other rock types became common, or came into being: blueschist, coal, and bioclastic limestone. Through it all, sea level fluctuated via a complex interplay of ridge volume, glaciation, and positions of ocean basins and continents over geoid highs and lows. Only the Pangea cycle can be understood in the context of Earth processes as they operate today.

Every secular trend can have only one correct explanation, complicated though it might be. Moreover, because the Earth has only one history, any viable explanation for one secular trend must honor all the rest. An encyclopedic approach is indicated.

Acknowledgments

I am grateful to reviewers Alison Till, Francis Macdonald, Kent Condie, Rich Goldfarb, and Alfred Kröner for their many constructive suggestions. This paper grew out of the 2004 Penrose Conference on Secular Variation in Tectonics and Allied Fields ([Bradley and Dewey, 2005](#)), which received support from the USGS Venture Capital Fund. The global perspective needed for this kind of synthesis came from Kevin Burke and John Dewey. Theresa Taylor, Heather Bleick, and Sam Friedman helped with the detrital zircon compilation. I benefited from various discussions and exchanges with Wouter Bleeker, Mike Brown, Bill Collins, Puol Emsbo, David Evans, Rich Goldfarb, Peter Haessler, Paul Hoffman, Karl Karlstrom, Dave Leach, Andrew McCauley, Joe Meert, Greg Retallack, Celal Sengör, Graham Shields, Paul Silver, Bob Stern, Jan Veizer, Maarten de Wit, and many others. Gerard Stampfli provided the plate reconstructions in Fig. 1; Ian Campbell provided data tables used to construct Fig. 15; Kent Condie provided data tables

used to construct Fig. 14 and A43–A48, and Christ Hawkesworth and Bruno Dhuime provided a high resolution version of Figure A36.

Appendix A. Supplementary data

Supplementary data to this article can be found online at [doi:10.1016/j.earscirev.2011.05.003](https://doi.org/10.1016/j.earscirev.2011.05.003).

References

- Allegre, C., Manhès, G., Lewin, E., 2001. Chemical composition of the Earth and the volatility control on planetary genetics. *Earth and Planetary Science Letters* 185, 49–69.
- Ashwal, L.D., 1993. *Anorthosites*. Springer-Verlag, Berlin, 422 p.
- Barley, M.E., Groves, D.I., 1992. Supercontinent cycles and the distribution of metal deposits through time. *Geology* 20, 291–294.
- Bekker, A., Slack, J.F., Planavsky, N., Krapež, B., Hofmann, A., Konhauser, K.O., Rouxel, O.J., 2010. Iron formation: the sedimentary product of a complex interplay among mantle, tectonic, oceanic, and biospheric process. *Economic Geology* 105, 467–508.
- Bennett, V.C., 2003. Compositional evolution of the mantle. *Treatise on Geochemistry* 2, 493–519.
- Bleeker, W., 2003. The late Archean record: a puzzle in ca. 35 pieces. *Lithos* 71, 99–134.
- Bradley, D.C., 2008. Passive margins through earth history. *Earth-Science Reviews* 91, 1–26.
- Bradley, D.C., Leach, D.L., 2003. Tectonic controls of Mississippi Valley-type lead-zinc mineralization in orogenic forelands. *Mineralium Deposita* 38, 652–667.
- Bradley, D.C., Dewey, J.F., 2005. Penrose conference report: secular variation in tectonics and allied fields. *GSA Today* 15 (3), 12.
- Brown, M., 2007. Metamorphic conditions in orogenic belts: a record of secular change. *International Geology Review* 49, 193–234.
- Brown, M., 2008. Characteristic thermal regimes of plate tectonics and their metamorphic imprint throughout Earth history: when did Earth first adopt a plate tectonics mode of behavior? *Geological Society of America Special Paper* 440, 97–128.
- Burke, K., Dewey, J.F., Kidd, W.S.F., 1976. Dominance of horizontal movements, arc and microcontinental collisions during the later Permian Regime. In: Windley, B.F. (Ed.), *The Early History of the Earth*. John Wiley & Sons, New York, pp. 113–130.
- Burke, K., Ashwal, L.D., Webb, S., 2003. New way to map old sutures using deformed alkaline rocks and carbonatites. *Geology* 31, 391–394.
- Campbell, I.H., Allen, C.M., 2008. Formation of supercontinents linked to increases in atmospheric oxygen. *Nature Geoscience* 1, 554–558. [doi:10.1038/ngeo259](https://doi.org/10.1038/ngeo259).
- Cawood, P.A., Suhr, G., 1992. Generation and obduction of ophiolites: constraints from the Bay of Islands Complex, western Newfoundland. *Tectonics* 11, 884–897.
- Cogley, J.G., 1984. Continental margins and the extent and number of continents. *Reviews of Geophysics and Space Physics* 22, 101–122.
- Collins, W.J., 2003. Slab pull, mantle convection, and Pangaean assembly and dispersal. *Earth and Planetary Science Letters* 205, 225–237.
- Condie, K.C., 1994. Greenstones through time. *Developments in Precambrian Geology* 11, 85–120.
- Condie, K.C., 1997. *Plate Tectonics and Crustal Evolution*, 4th edition. Butterworth-Heinemann, Boston, 282 p.
- Condie, K.C., 2003. Supercontinents, superplumes and continental growth: the Neoproterozoic record. *Geological Society of London Special Publications* 206, 1–21.
- Condie, K.C., 2005. *Earth as an Evolving Planetary System*. Elsevier Academic Press, Amsterdam, 447 p.
- Condie, K.C., O'Neill, C., 2010. The Archean-Proterozoic boundary: 500 My of tectonic transition in Earth history. *American Journal of Science* 310, 775–790.
- Condie, K.C., Belousova, E., Griffin, W.L., Sircombe, K.N., 2009a. Granitoid events in space and time: constraints from igneous and detrital zircon age spectra. *Gondwana Research* 15, 228–242.
- Condie, K.C., O'Neill, C., Aster, R.C., 2009b. Evidence and implications for a widespread magmatic shutdown for 250 My on Earth. *Earth and Planetary Science Letters* 282, 294–298.
- Condie, K.C., Bickford, M.E., Aster, R.C., Belousova, E., Scholl, D.W., 2011. Episodic zircon ages. Hf isotopic composition and the preservation rate of continental crust. *Geological Society Bulletin*. 123, 951–957.
- de Wit, M.J., and Ashwal, L.D., 1997. Convergence towards divergent models of greenstone belts. In: M.J. de Wit and L.D. Ashwal (Eds.), *Greenstone Belts*: Oxford University Press, New York, p. ix–xix.
- Dewey, J.F., 2007. The secular evolution of plate tectonics and the continental crust: an outline. *Geological Society of America Memoir* 200, 1–7. [doi:10.1130/2007.1200\(01\)](https://doi.org/10.1130/2007.1200(01)).
- Dewey, J.F., Burke, K., 1974. Hotspots and continental breakup: implications for collisional orogeny. *Geology* 2, 57–60.
- Dilek, Y., 2003. Ophiolite pulses, orogeny, and mantle plumes. *Geological Society of London Special Publications* 218, 9–19.
- Domagal-Goldman, S.D., Kasting, J.F., Johnston, D.T., Farquhar, J., 2008. Organic haze, glaciations and multiple sulfur isotopes in the Mid-Archean Era. *Earth and Planetary Science Letters* 269, 29–40.
- Evans, D.A.D., 2009. The paleomagnetically viable, long-lived and all-inclusive Rodinia supercontinent reconstruction. *Geological Society, London, Special Publications* 327, 371–404.

- Eyles, N., 2008. Glacio-epochs and the supercontinent cycle after ~3.0 Ga: tectonic boundary conditions for glaciation. *Palaeogeography, Palaeoclimatology, Palaeoecology* 258, 89–129.
- Farquhar, J., Wu, N., Canfield, D.E., Oduro, H., 2010. Connections between sulfur cycle evolution, sulfur isotopes, sediments, and base metal sulfide deposits. *Economic Geology* 105, 509–533.
- Garrels, R.M., Mackenzie, F.T., 1971. *Evolution of Sedimentary Rocks*. Norton, New York, 397 p.
- Goldfarb, R.J., Groves, D.I., Gardoll, S., 2001a. Orogenic gold and geologic time: a global synthesis. *Ore Geology Reviews* 18, 1–75.
- Goldfarb, R.J., Bradley, D.C., Leach, D.L., 2010. Secular variation in economic geology. *Economic Geology* 105, 459–465.
- Gradstein, F.M., Ogg, J.G., 2004. *A geologic time scale 2004*. Cambridge University Press, Cambridge, 598 p., 1 plate.
- Griffin, W.L., O'Reilly, S.Y., Abe, N.S., Aulbach, S., Davies, R.M., Pearson, N.J., Doyle, B.J., Kivi, K., 2003. The origin and evolution of Archean lithospheric mantle. *Precambrian Research* 127, 19–41.
- Griffin, W.L., O'Reilly, S.Y., Afonso, J.C., Begg, G.C., 2009. The composition and evolution of lithospheric mantle: a re-evaluation and its tectonic implications. *Journal of Petrology* 50, 1185–1204.
- Grove, T.L., Parman, S.W., 2004. Thermal evolution of the Earth as recorded by komatiites. *Earth and Planetary Science Letters* 219, 173–187.
- Groves, D.I., Condie, K.C., Goldfarb, R.J., Hronsky, J.M.A., Vielreicher, R.M., 2005. Secular changes in global tectonic processes and their influence on the temporal distribution of gold-bearing mineral deposits. *Economic Geology* 100, 203–224.
- Hallam, A., 1992. *Phanerozoic Sea-Level Changes*. Columbia University Press, New York, 266 p.
- Haq, B.U., Schutter, S.R., 2008. A chronology of Paleozoic sea-level changes. *Science* 322, 64–68. doi:10.1126/science.1161648.
- Haq, B.U., Hardenbol, J., Vail, P.R., 1987. Chronology of fluctuating sea levels since the Triassic. *Science* 235 (4793), 1156–1167. doi:10.1126/science.235.4793.1156.
- Hargraves, R.B., 1986. Faster spreading or greater ridge length during the Archean? *Geology* 14, 750–752.
- Hawkesworth, C.J., Dhuime, B., Pietranik, A.B., Cawood, P.A., Kemp, A.I.S., Storey, C.D., 2010. The generation and evolution of the continental crust. *Journal of the Geological Society, London* 167, 229–248. doi:10.1144/0016-76492009-072.
- Hays, J.D., Pitman III, W.C., 1973. Lithospheric plate motion, sealevel changes and climatic and ecological consequences. *Nature* 246, 18–22.
- Heller, P.L., Angevine, C.L., 1985. Sea-level cycles and the growth of Atlantic-type oceans. *Earth and Planetary Science Letters* 75, 417–426.
- Herzberg, C., Condie, K., Korenaga, J., 2010. Thermal history of the Earth and its petrological expression. *Earth and Planetary Science Letters* 292, 79–88.
- Hoffman, P.F., 1987. Early Proterozoic foredeeps, foredeep magmatism, and superior-type iron-formation of the Canadian shield. *American Geophysical Union Geodynamics Series* 17, 85–98.
- Hoffman, P.F., 1989. Speculations on Laurentia's first big year (2.0 to 1.0 Ga). *Geology* 17, 135–138.
- Hoffman, P.F., 1991. Did the breakout of Laurentia turn Gondwana inside out? *Science* 252, 1409–1412.
- Hoffman, P.F., 1997. Tectonic genealogy of North America. In: van der Pluijm, B.A., Marshak, S. (Eds.), *Earth Structure: an Introduction to Structural Geology and Tectonics*. McGraw-Hill, New York, pp. 459–464.
- Hoffman, P.F., 1999. The break-up of Rodinia, birth of Gondwana, true polar wander and the snowball Earth. *Journal of African Earth Sciences* 17, 17–33.
- Hoffman, P.F., 2009. Pan-Glacial—a third state in the climate system. *Geology Today* 25, 100–107.
- Huston, D.L., Logan, G.A., 2004. Barite, BIFs and bugs: evidence for the evolution of the Earth's early hydrosphere. *Earth and Planetary Science Letters* 220, 41–55.
- Isley, A.E., Abbott, D.H., 1999. Plume-related mafic volcanism and the deposition of banded iron formation. *Journal of Geophysical Research* 104, 5461–5477.
- Isley, A.E., Abbott, D.H., 2002. The intensity, occurrence, and duration of superplume events and eras over geologic time. *Journal of Geodynamics* 34, 265–307.
- Karlstrom, K.E., Ahall, K.-I., Harlan, S.S., Williams, M.L., McClelland, J., Geissman, J.W., 2001. Long-lived (1.8–1.0 Ga) convergent orogen in southern Laurentia, its extensions to Australia and Baltica, and implications for refining Rodinia. *Precambrian Research* 111, 5–30.
- Korenaga, J., 2006. Archean geodynamics and thermal evolution of Earth: Archean geodynamics and environments. *AGU Geophysical Monograph Series* 164, 7–32.
- Kröner, A., Layer, P., 1992. Crust formation and plate motion in the early Archean. *Science* 256, 1405–1411.
- Leach, D.L., Bradley, D.C., Pisarevsky, S.A., Taylor, R.D., Gardoll, S.J., 2010. The genesis of sediment-hosted lead-zinc deposits in Earth history. *Economic Geology* 105, 593–625.
- Li, Z.-X., Bogdanova, S.V., Collins, A.S., Davidson, A., DeWaele, B., Ernst, R.E., Fitzsimons, I.C.W., Fuck, R.A., Gladkochub, D.P., Jacobs, J., Karlstrom, K.E., Lu, S., Natapov, L.M., Pease, V., Pisarevsky, S.A., Thrane, K., Vernikovsky, V., 2008. Assembly, configuration, and break-up history of Rodinia: a synthesis. *Precambrian Research* 160, 179–210.
- Meyer, C., 1981. Ore-forming processes in geologic history of the earth. *Economic Geology*, pp. 6–41. 75th Anniversary Volume.
- Meyer, C., 1988. Ore deposits as guides to geologic history of the earth. *Annual Reviews of Earth Science* 16, 147–171.
- Moore, E.M., 1991. Southwest US-East Antarctic (SWEAT) connection: a hypothesis. *Geology* 19, 425–428.
- Moore, E.M., 2002. Pre-1 Ga (pre-Rodinian) ophiolites: their tectonic and environmental implications. *GSA Bulletin* 114, 80–95.
- Murphy, J.B., Nance, R.D., 2003. Do supercontinents introvert or extrovert? Sm-Nd isotope evidence. *Geology* 31, 873–876.
- Murphy, J.B., Nance, R.D., 2007. Do supercontinents turn inside-in or inside-out? *International Geology Review* 47, 591–619.
- Nance, R.D., Worsley, T.R., Moody, J.B., 1986. Post-Archean biogeochemical cycles and long-term episodicity in tectonic processes. *Geology* 14, 514–518.
- Parkinson, C.D., Motoki, A., Onishi, C.E., Maruyama, S., 2001. Ultrahigh-pressure pyrope kyanite granulites and associated eclogites in Neoproterozoic nappes of Southeast Brazil. [abs.] UHPM Workshop 2001, Fluid/slab/mantle interactions and ultrahigh-P minerals. Waseda University, Tokyo, pp. 87–90. Abstract Volume.
- Pollack, H.N., 1997. Thermal characteristics of the Archean. In: De Wit, M.J., Ashwal, L.D. (Eds.), *Greenstone Belts*. Clarendon Press, Oxford, pp. 223–232.
- Poudjom Djomani, Y.H., O'Reilly, S.Y., Griffin, W.L., Morgan, P., 2001. The density structure of subcontinental lithosphere through time. *Earth and Planetary Science Letters* 184, 605–621.
- Prokoph, A., Ernst, R.E., Buchan, K.L., 2004. Time-series analysis of Large Igneous Provinces: 3500 Ma to present. *Journal of Geology* 112, 1–22.
- Reddy, S.A., Evans, D.A.D., 2009. Palaeoproterozoic supercontinents and global evolution: correlations from core to atmosphere. *Geological Society, London, Special Publication* 323, 1–26.
- Richter, F.M., Rowley, D.B., DePaolo, D.J., 1992. Sr isotopic evolution of seawater: the role of tectonics. *Earth and Planetary Science Letters* 109, 11–23.
- Rino, S., Kon, Y., Sato, W., Maruyama, S., Santosh, M., Zhao, D., 2008. The Grenvillian and Pan-African orogens: world's largest orogenies through geologic time, and their implications on the origin of superplume. *Gondwana Research* 14, 51–72.
- Rogers, J.J.W., Santosh, M., 2002. Configuration of Columbia, a Mesoproterozoic supercontinent. *Gondwana Research* 5, 5–22.
- Rogers, J.J.W., Santosh, M., 2003. Supercontinents in Earth history. *Gondwana Research* 6, 357–368.
- Ronov, A.B., Yaroshevskiy, A.A., Migdisov, A.A., 1991. Chemical constitution of the Earth's crust and geochemical balance of the major elements (Part I). *International Geology Review* 33, 941–1097.
- Rowley, D.B., 2002. Rate of plate creation and destruction: 180 Ma to present. *Geological Society of America Bulletin* 114, 927–933.
- Rukhlov, A.S., Bell, K., 2010. Geochronology of carbonates from the Canadian and Baltic Shields, and the Canadian Cordillera: clues to mantle evolution. *Mineralogy and Petrology* 98, 11–54. doi:10.1007/s00710-009-0054-5.
- Slater, J.G., Jaupart, C., Galson, D., 1980. The heat flow through oceanic and continental crust and the heat loss of the Earth. *Reviews of Geophysics and Space Physics* 18, 269–311.
- Scotese, C.R., 1997. *Continental Drift Flip Book*, 7th edition. Arlington, Texas, 80 p.
- Scott, C., Lyons, T.W., Bekker, A., Shen, Y., Poulton, S.W., Chu, X., Anbar, A.D., 2008. Tracing the stepwise oxygenation of the Proterozoic ocean. *Nature* 452, 456–459.
- Sears, J.W., Price, R.A., 2003. Tightening the Siberian connection to western Laurentia. *Geological Society of America Bulletin* 115, 943–953.
- Sengör, A.M.C., Altiner, D., Cin, A., Ustaömer, T., Hsu, K.J., 1988. Origin and assembly of the Tethyside orogenic collage at the expense of Gondwana Land. *Geological Society of London Special Publication* 37, 119–181.
- Shields, G.A., 2007. A normalised seawater strontium isotope curve: possible implications for Neoproterozoic–Cambrian weathering rates and the further oxygenation of the Earth. *eEarth* 2, 35–42.
- Shields, G., Veizer, J., 2002. Precambrian marine carbonate isotope database: version 1.1. *Geochemistry, Geophysics, Geosystems* 6, 1–12.
- Silver, P.G., Behn, M.D., 2008. Intermittent plate tectonics. *Science* 319, 85–88.
- Slack, J.F., Cannon, W.F., 2008. Shifts in global metallogeny at 1850 Ma: a connection to the giant Sudbury impact event? *Geological Society of America Abstracts with Programs* 40 (6), 146.
- Stampfli, G.M., Borel, G.D., 2002. A plate tectonic model for the Paleozoic and Mesozoic constrained by dynamic plate boundaries and restored synthetic oceanic isochrons. *Earth and Planetary Science Letters* 196, 17–33.
- Stampfli, G., Marcoux, J., Baud, A., 1991. Tethyan margins in space and time. *Palaeogeography, Palaeoclimatology, Palaeoecology* 87, 373–409.
- Veizer, J., Jansen, S.L., 1979. Basement and sedimentary recycling and continental evolution. *Journal of Geology* 87, 341–370.
- Veizer, J., Jansen, S.L., 1985. Basement and sedimentary recycling: 2. Time dimension to global tectonics. *Journal of Geology* 93, 625–643.
- Veizer, J., Mackenzie, F.T., 2003. Evolution of sedimentary rocks. *Treatise on Geochemistry* 7, 369–407.
- Veizer, J., Laznicka, P., Jansen, S.L., 1989. Mineralization through geologic time: recycling perspective. *American Journal of Science* 289, 484–524.
- Vervoort, J.D., Patchett, P.J., Blichert-Toft, J., Albarede, F., 1999. Relationships between Lu–Hf and Sm–Nd isotopic systems in the global sedimentary system. *Earth and Planetary Science Letters* 168, 79–99.
- Whitmeyer, S.J., Karlstrom, K.E., 2007. Tectonic model for the Proterozoic growth of North America. *Geosphere* 3, 220–259. doi:10.1130/GES00055.
- Williams, H., Hoffman, P.H., Lewry, J.F., Monger, J.W.H., Rivers, T., 1991. Anatomy of North America: thematic geologic portrayals of the continents. *Tectonophysics* 187, 117–134.
- Wilson, J.T., 1968. Static or mobile Earth: the current scientific revolution. *Proceedings of the American Philosophical Society* 112, 309–320.
- Woolley, A.R., Kjargaard, B.A., 2008. Carbonate occurrences of the world: map and database. *Geological Survey of Canada Open File* 5796, 1 CD-ROM + 1 map.
- Worsley, T.R., Nance, R.D., Moody, J.B., 1984. Global tectonics and eustasy for the past 2 billion years. *Marine Geology* 58, 373–400.
- Worsley, T.R., Nance, R.D., Moody, J.B., 1986. Tectonic cycles and the history of the earth's biogeochemical and paleoceanographic record. *Paleoceanography* 1, 233–263.
- Zhao, G., Cawood, P.A., Wilde, S.A., Sun, M., 2002. Review of global 2.1–1.8 Ga orogens: implications for a pre-Rodinia supercontinent. *Earth Science Reviews* 59, 125–162.

Supplementary Data For:
**Secular trends in the geologic record
and the supercontinent cycle¹**

Dwight C. Bradley

*U.S. Geological Survey, 4200 University Drive, Anchorage, Alaska 99508 U.S.A.
dbradley@usgs.gov*

Additional discussion of secular trends plotted in Figures 3-45.

This electronic-only supplement provides additional information about the secular trends featured in the main body of the paper, with particular emphasis on secular trends that are new to this paper. Compilations covering the whole Earth and all of geologic time are not easy. If broader inferences are to be based these secular trends, it is important that their strengths and weaknesses be acknowledged.

Indices of supercontinentality (supplement to Section 4.1)

The aim of Figures 3 and 4 is to quantify what is plainly seen in a sequence of Phanerozoic paleogeographic maps: that the continents were dispersed, then gathered into a single supercontinent, and then dispersed once again. In Figure 3, the y axis is shown in square kilometers and in percentage of total continental area, using 214 million km sq for the total (from Cogley, 1984).

Passive margins (supplement to Sections 4.2 and 6.2)

Figures 11, 12, 13, 27, and 28 are from my recent synthesis of passive margins through time (Bradley, 2008). A lengthy online appendix included writeups of each passive margin that gave reasons for the tectonic interpretation, and for the ages picked for the start date and end date (rift-drift transition and onset of collision). The dataset is a distillation of the tectonic interpretations of >80 passive margins in orogenic belts. Undoubtedly, mistaken interpretations were included—such is the difficulty of unraveling orogenic histories—but the overall form of the passive margin age distribution (Fig. 11) is probably robust. Each passive margin was assigned a quality ranking from A to D, based on my confidence in the tectonic interpretation and my perception of the reliability of the age control. Passive margins of each quality group have similar age distributions. In the passive-margin record, the interval from ca. 1650 to ca. 1050 Ma is problematic because the tectonic interpretations are debatable and the age controls are poor on the few putative margins of that age. The plot of passive-margin lifespans (Fig. 27) has greater potential for error (Bradley, 2008). Figure 28 is new and derived from the lifespan data. By analogy with the modern passive margins, each ancient passive margin is assumed to have been flanked by seafloor that, by definition, has the same age as the "start date" of the margin. Thus the end date minus the start date gives the age of that strip of oceanic crust at the time that it was subducted, just before the start of collision. In Figure 27, the x-value is the start date, and the y-value is the lifespan.

Orogenic granites and detrital zircons (supplement to Sections 4.3 and 6.9)

The plot of zircon ages from orogenic granites in Fig. 14 (from appendix in Condie et al., 2009a) is the most recent iteration of a series of such plots by Condie. Some reasons for the paucity of Phanerozoic ages were discussed in Section 4.2. Another reason is that the ⁴⁰Ar/³⁹Ar method is widely used instead of the U-Pb method for Mesozoic and younger igneous rocks, so zircon ages are not reported. In an earlier version (Fig. A19), Condie (1997) used (but did not fully describe) a weighting procedure designed not to over-represent well-studied igneous belts. Condie's plots improve on earlier plots of the same type by Gastil (1960), Hurley and Rand (1969), and Glikson (1983; Fig. A20). Those early plots were largely based on K/Ar and Rb/Sr data that

¹ Bradley, D.C., 2011. Secular trends in the geologic record and the supercontinent cycle. Earth-Science Reviews. DOI: 0.1016/j.earscirev.2011.05.003

would not meet today's standards of precision or accuracy. In addition, many more age determinations are now available, and this is especially important because remote parts of the world were poorly represented in the earlier tallies. Despite these differences in methodology, the major peaks in Figure 14 were already evident by 1960.

Two plots are shown of detrital zircons from modern river sands (Figs. 15 and A21). The advantage of this method is in capturing zircon populations from broad regions in a small number of samples. Potential shortcomings of the detrital record include (1) destruction of high-U zircons in transit from bedrock source to river delta, (2) under-representation of small zircons, (3) over-representation of plutonic sources that are anomalously rich in zircon, (4) over-representation of zircons from areas of rapid erosion, and (5) sampling bias against young orogens and magmatic arcs. A study designed to incorporate and properly weight data from smaller rivers would be useful.

Figure 16 is a new plot based on my own compilation of detrital zircons of the world. It is far from complete and could be much improved by devising a way to guard against undue influence of data from heavily sampled regions. In Figure 40, the >26,000 igneous ages have been plotted as a function of the depositional age of the host sandstone or metasediment. Each data point that plots below the diagonal line is in the forbidden zone: either the true depositional age is younger than shown, the true zircon age is older, or both.

(Note added in proof: Voice et al. (2011) published a new compilation of about 200,000 detrital zircon ages after final version of the present paper was submitted. The maxima and minima are similar to those shown in Figures 14-16.)

Metamorphic rocks (supplement to Sections 4.6 and 6.4)

The histograms showing occurrences of blueschist, granulite-, and eclogite-facies metamorphism (Figs. 20, 21, and 30) were constructed from data tables in Brown (2007). The plots of metamorphic pressures and geothermal gradient (Figs. 31 and 32) were redrafted from Brown (2008). Brown (2008) argued that the coeval existence of two distinctive P-T regimes as far back as the Neoproterozoic is an earlier manifestation of the classic paired metamorphic belts of the Phanerozoic, and constitutes evidence for plate tectonics.

Carbonatites (supplement to Section 4.7)

The histogram in Figure 22 was plotted from an Excel table in Woolley and Kjarsgaard (2008). The published histogram in that paper was binned in 75-m.y. increments. Only about half of the carbonatites listed in Woolley and Kjarsgaard's comprehensive study were assigned an age.

Large Igneous Provinces (supplement to Section 4.8)

The age distribution of ancient LIPs (Fig. 23) is based on occurrences of flood basalts, layered mafic intrusions, mafic dike swarms, and komatiites. A komatiite need not be regionally extensive to count; that is, the "large" in Large Igneous Province is not a prerequisite for this census. An arc origin for any of the komatiites (e.g., Grove and Parman, 2004) would exaggerate the LIP record before about 1800 Ma.

Oceanic crust and ophiolites (supplement to Sections 6.2 and 6.3)

Figure 8 was adapted from Sclater et al. (1980). The original plot employed bins of somewhat uneven duration corresponding to the subdivisions of the Mesozoic-Cenozoic time scale as it stood in 1980; the bins have been resized in the x-dimension to conform to the Gradstein and Ogg (2004) time scale.

Figure 29 was pieced together from compilations by Dilek (2003) for ophiolites between 0 and 1000 Ma, and from Moores (2002) for ophiolites from 1000 to ca. 3500 Ma. Moores (2002) provided a summary data table, whereas Dilek did not, making it harder to merge the two datasets. Dilek (2003) plotted the age distribution of ophiolites in histogram form but with uneven bin sizes: in the Phanerozoic, bins appear to correspond to various uneven divisions of a geologic time scale that predates Gradstein and Ogg (2004), perhaps 5 to 15 m.y. in duration, whereas bins in the Neoproterozoic appear to be 20 m.y. wide. To more faithfully portray the merged data, everything in Figure 29 has been replotted in 50 m.y. bins. A few Phanerozoic and Neoproterozoic ophiolites may have been inadvertently assigned to the next-adjacent bin in the process. In those cases where Moores (2002) gave an age range, I used the midpoint.

Mantle-derived igneous rocks (supplement to Section 6.5)

Plots of density, mineralogy, and chemistry of average subcontinental lithospheric mantle through time (Figs. 35, A27, and A28) were derived from data tables in Poudjom Djomani et al. (2001) and Griffin et al. (2003). The xenoliths analyzed in these studies were assumed to be about the same age as the upper crust into which they were emplaced. Age groupings are so broad that only generalized, first-order trends can be detected.

A schematic plot of mantle redox conditions by Delano (2001) is shown in Figure A35. The mantle's oxidation state was inferred from whole-rock abundances of Cr and V in ancient volcanics, and from the composition of Cr-rich spinels in ancient volcanics. This study was based on samples whose ages were only broadly assigned (e.g. Archean, Proterozoic, etc.). The oxidation state of the mantle has remained constant since the Eoarchean. The suggestion that oxidation of the atmosphere at around the Archean-Proterozoic boundary was due to a mantle overturn event (Kump et al., 2001) is therefore untenable.

Massif anorthosites (supplement to Section 6.6)

The histogram in Figure 27 was constructed from tabulated data in Ashwal (1993). Anorthosites having age assignments with errors >50 m.y. were excluded. Given the worldwide advancement of zircon geochronology since the early 1990s, it would be worth updating this plot.

Sedimentary recycling (supplement to Section 6.9)

Each sedimentary rock analyzed is a mix of clastic grains from various sources, so each data point represents an average, at a given time, of crustal residence ages from the sediment catchment area. The red line is $x = y$ and below it is the forbidden zone. Hafnium isotopes from sediments show essentially the same age distribution as neodymium isotopes (Fig. A63). The new plot of igneous age versus depositional age (Fig. 40) is based on the global compilation of >26,000 detrital zircons shown in Figure 16. The clustering of data in Figures 39 and 40 is probably due to the disproportionate abundance of strata dating from times of supercontinent disassembly and assembly.

Sea level (supplement to Section 6.12)

An alternative to Hallam's (1992) sea level curve has been produced by Haq et al. (1987) for the latter half of the Phanerozoic, and Haq and Schuller (2008) for the earlier half. The curves are broadly in agreement but differ in some details.

References cited in Appendix only

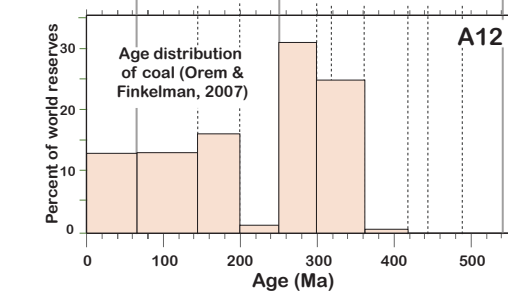
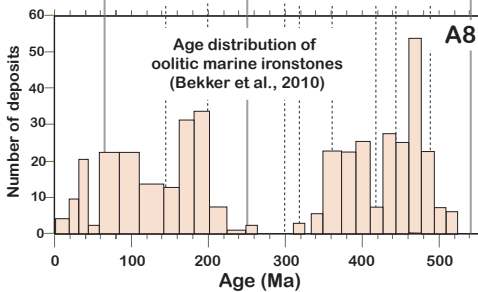
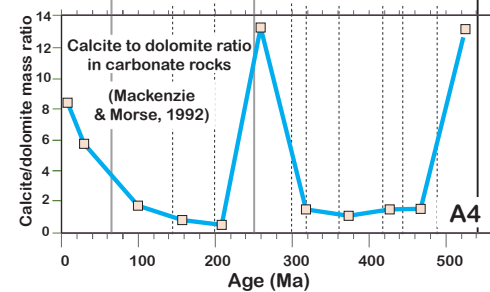
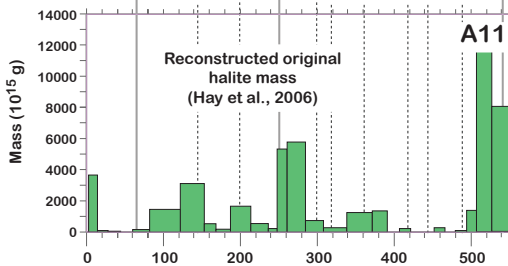
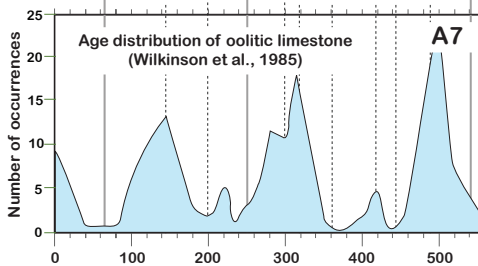
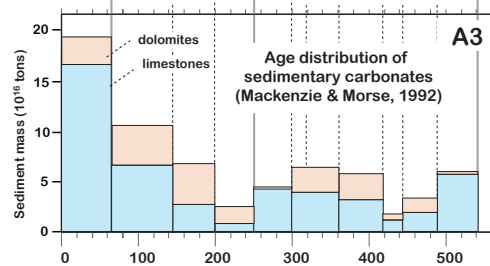
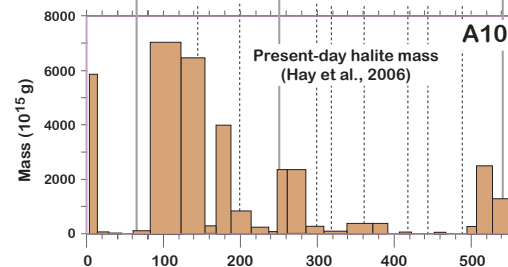
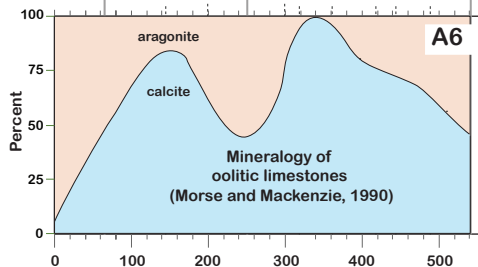
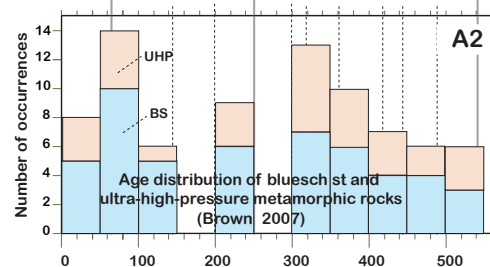
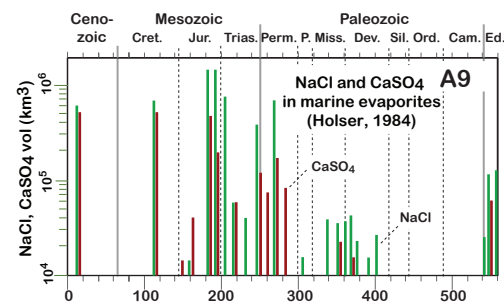
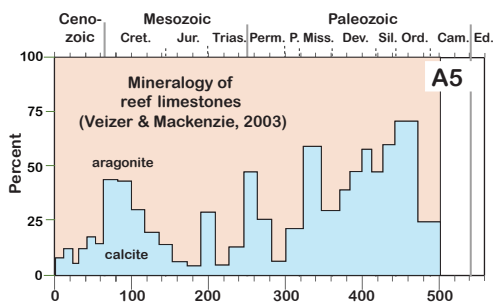
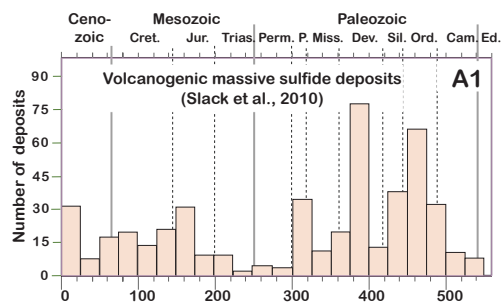
- Abbott, D.H., and Isley, A.E., 2002. Extraterrestrial influences on mantle plume activity. *Earth and Planetary Science Letters* 205, 53-62.
- Artemieva, I.M., and Mooney, W.D., 2001. Thermal thickness and evolution of Precambrian lithosphere: A global study. *Journal of Geophysical Research* 106, 16387-16414.
- Artemieva, I.M., and Mooney, W.D., 2002. On the relations between cratonic lithosphere thickness, plate motions, and basal drag. *Tectonophysics* 358, 211-231.
- Bekker, A., Slack, J.F., Planavsky, N., Krapež, B., Hofmann, A., Konhauser, K.O., and Rouxel, O.J., 2010. Iron formation: the sedimentary product of a complex interplay among mantle, tectonic, oceanic, and biospheric process. *Economic Geology* 105, 467-508.
- Bois, C., Bouche, P., and Pelet, R., 1982. Global geologic history and distribution of hydrocarbon reserves. *American Association of Petroleum Geologists Bulletin* 66, 1248-1270.
- Condie, K.C., 2003b. Incompatible element ratios in oceanic basalts and komatiites: Tracking deep mantle sources and continental growth rates with time. *Geochemistry, Geophysics, Geosystems* 4, 1-28.
doi:10.1029/2002GC000333.

- Condie, K.C., 2008. Did the character of subduction change at the end of the Archean? Constraints from convergent-margin granitoids. *Geology* 36, 611-614.
- Condie, K.C., Des Marais, D.J., and Abbott, D., 2001. Precambrian superplumes and supercontinents: a record in black shales, carbon isotopes, and paleoclimates? *Precambrian Research* 106, 239-260.
- de Wit, M.J., and Ashwal, L.D., 1997, Convergence towards divergent models of greenstone belts, in M.J. de Wit and L.D. Ashwal, editors, *Greenstone Belts*: Oxford University Press, New York, p. ix-xix.
- Delano, J.W., 2001. Redox history of the earth's interior since ~3900 Ma: Implications for prebiotic molecules. *Origins of life and evolution of the Biosphere* 31, 311-341.
- Dunlap, W.J., 2000. Nature's diffusion experiment: The cooling-rate cooling-age correlation. *Geology* 28, 139-142.
- Durrheim, R. J., and Mooney, W.D., 1994. Evolution of the Precambrian Lithosphere: Seismological and geochemical constraints. *Journal of Geophysical Research* 99, 15359-15374.
- Evans, D.A.D., 2006. Proterozoic low orbital obliquity and axial-dipolar geomagnetic field from evaporite palaeolatitudes. *Nature*, 444, 51-55.
- Gastil, G., 1960. The distribution of mineral dates in space and time. *American Journal of Science* 258, 1-35.
- Glikson, A.Y., 1983. Geochemical, isotopic, and paleomagnetic tests of early sial-sima patterns; the Precambrian crustal enigma revisited, *in* Medaris, L.G., Jr., Byers, C.W., Mickelson, D.M., and Shanks, W.C., editors, *Proterozoic geology; selected papers from an international Proterozoic symposium*. Geological Society of America Memoir 161, 95-117.
- Gough, D.O., 1981. Solar interior structure and luminosity variations. *Solar Physics* 74, 21-34.
- Hartmann, W.K., Ryder, G., Dones, L., and Grinspoon, D., 2000. The time-dependent intense bombardment of the primordial Earth/Moon system, *in* R.M. Canup and K. Righter, editors, *Origin of the Earth and Moon*. Tucson, University of Arizona Press, 493-512.
- Hazen, R.M., Papineau, D., Bleeker, W., Downs, R.T., Ferry, J.M., McCoy, T.M., Sverjensky, D.A., and Yang, H., 2008. Mineral evolution. *American Mineralogist*, 93, 1693-1720.
- Holland, H. D., 2006. The oxygenation of the atmosphere and oceans. *Philosophical Transactions of the Royal Society B*, 361, 903-915.
- Jewell, P.W., 2000, Bedded barite in the geological record. *SEPM Special Publication* 66, 147-161.
- Johnson, C.M., Beard, B.L., and Roden, E.E., 2008. The iron isotope fingerprints of redox and biogeochemical cycling in modern and ancient Earth. *Annual Review of Earth and Planetary Sciences* 36, 457-493. doi: 10.1146/annurev.earth.36.031207.124139.
- Komiya, T., 2007. Material circulation through time; chemical differentiation within the mantle and secular variation of temperature and composition of the mantle, *In*: Yuen, D.A., Maruyama, S., Karato, S.-I., and Windley, B.F., (Eds.), *Superplumes: beyond plate tectonics*. Springer, Dordrecht, Netherlands, pp. 187-234.
- Kump, L.R., Kasting, J.F., and Barley, M.E., 2001. Rise of atmospheric oxygen and the "upside-down" Archean mantle: *Geochemistry Geophysics Geosystems* 2, Paper number 2000GC000114. ISSN: 1525-2027.
- Leach, D.L., Bradley, D.C., Pisarevsky, S.A., Taylor, R.D., and Gardoll, S.J., 2010. The genesis of sediment-hosted lead-zinc deposits in Earth history. *Economic Geology* 105, 593-625.

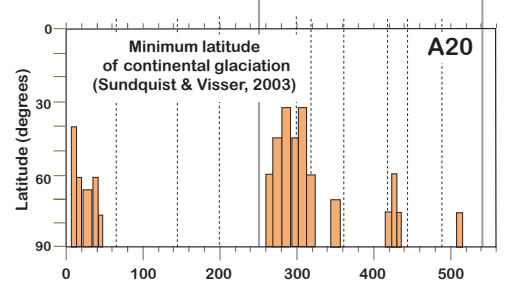
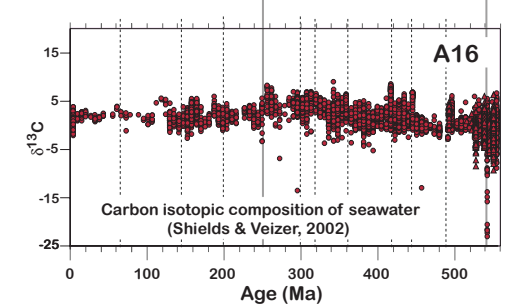
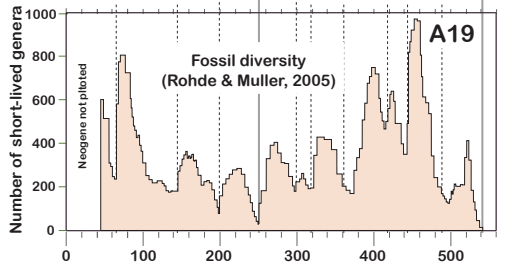
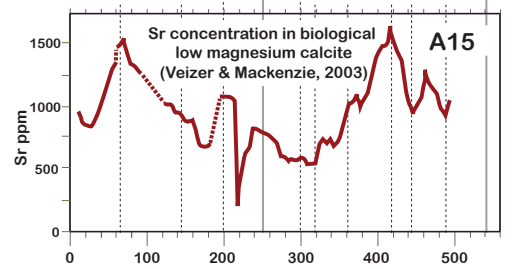
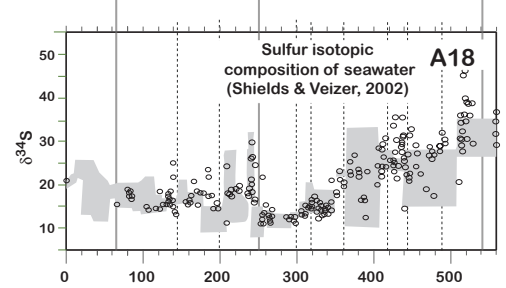
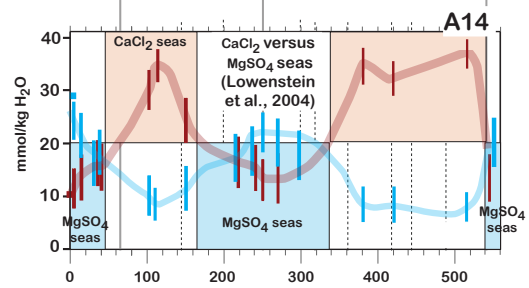
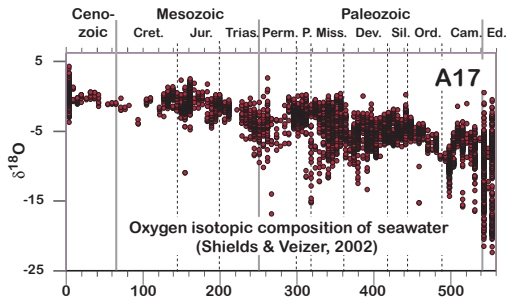
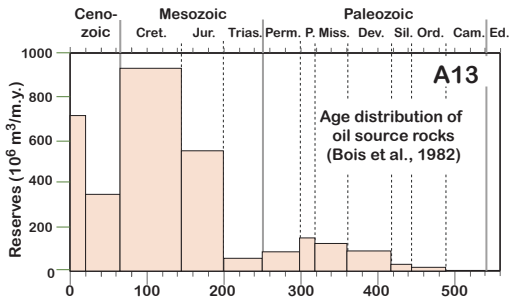
- Lowenstein, T.K., Hardie, L.A., Timofeeff, M.N., and Demicco, R.V., 2003. Secular variation in seawater chemistry and the origin of calcium chloride brines: *Geology* 31, 857-860.
- McLennan, Taylor, S.R., and Hemming, S.R., 2005. Composition, differentiation, and evolution of continental crust: constraints from sedimentary rocks and heat flow, *in* M. Brown and T. Rushmer, editors, *Evolution and Differentiation of the Continental Crust*, Cambridge University Press, 92-134.
- Muller, R. A., 2002. Measurement of the lunar impact record for the past 3.5 b.y. and implications for the Nemesis theory. *Geological Society of America Special Paper* 356, 659-665.
- Orem, W.H., and Finkelman, R.B., 2007. Coal Formation and Geochemistry. *Treatise of Geochemistry* 7, 191-222.
- Retallack, G.J., 2007. Coevolution of life and Earth. *Treatise of Geophysics* 9, 295-320.
- Rey, P.F., and Coultice, N., 2008. Neoproterozoic lithospheric strengthening and the coupling of Earth's geochemical reservoirs. *Geology* 36, 635-638.
- Rohde, R.A., and Muller, R.A., 2005. Cycles in fossil diversity. *Nature* 434, 208-210.
- Shaviv, N.J., 2003. The spiral structure of the Milky Way, cosmic rays, and ice age epochs on Earth. *New Astronomy* 8, 39-77.
- Sundquist, E.T., and Visser, K., 2003. The geologic history of the carbon cycle: *Treatise on Geochemistry* 8, 425-472.
- Taylor, S. R. and McLennan, S. M., 1985. *The continental crust: its composition and evolution*. Oxford, Blackwell Scientific Publications, 312 p.
- Tkachev, A.V., 2011. Evolution of metallogeny of granitic pegmatites associated with orogens throughout geological time. *Geological Society, London, Special Publications*, 350, 7-23
- Valley, J.W., Lackey, J.S., Cavosie, A.J., Clechenko, C.C., Spicuzza, M.J., Basei, M.A.S., Bindeman, I.N., Ferreira, V.P., Sial, A.N., King, E.M., Peck, W.H., Sinha, A.K., and Wei, C.S., 2005. 4.4 billion years of crustal maturation: oxygen isotope ratios of magmatic zircon. *Contributions to Mineralogy and Petrology* 150, 561-580. DOI 10.1007/s00410-005-0025-8.
- Voice, P.R., Kowalewski, M., and Eriksson, K.A., 2011. Quantifying the timing and rate of crustal evolution: global compilation of radiometrically dated detrital zircon grains. *Journal of Geology* 119, 109-126. DOI: 10.1086/658295

Figures A1-A86

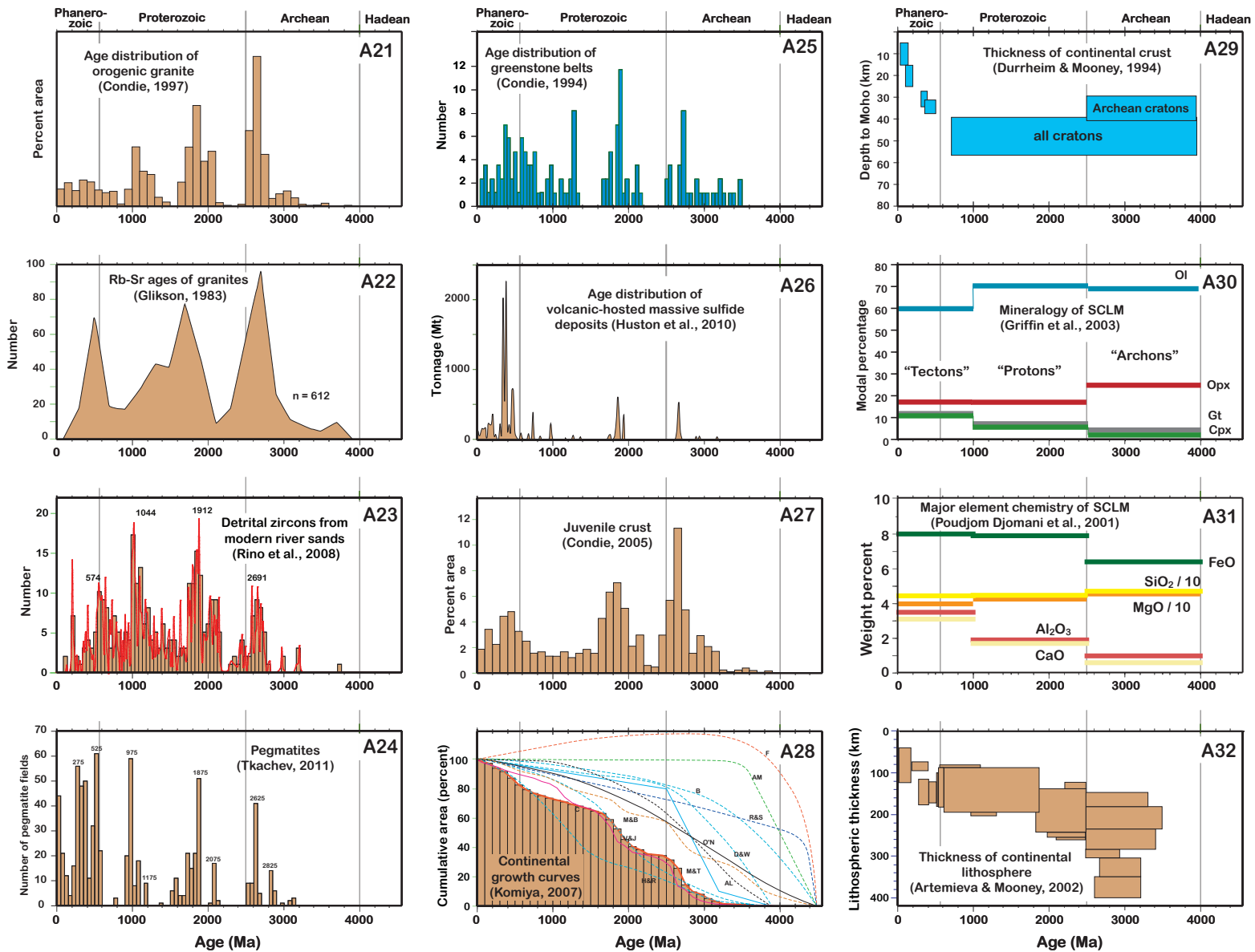
Figures A1-A86 show additional plots of secular trends that were compiled for this study and redrafted at the same scales as Figures 3-44. A few of these are redundant and a few others are of historical interest only—but most are in the Appendix because they bear only peripherally, if at all, on the supercontinent cycle. Table A1 summarizes the contents of Figures A1-A86 and takes the place of as many figure captions.



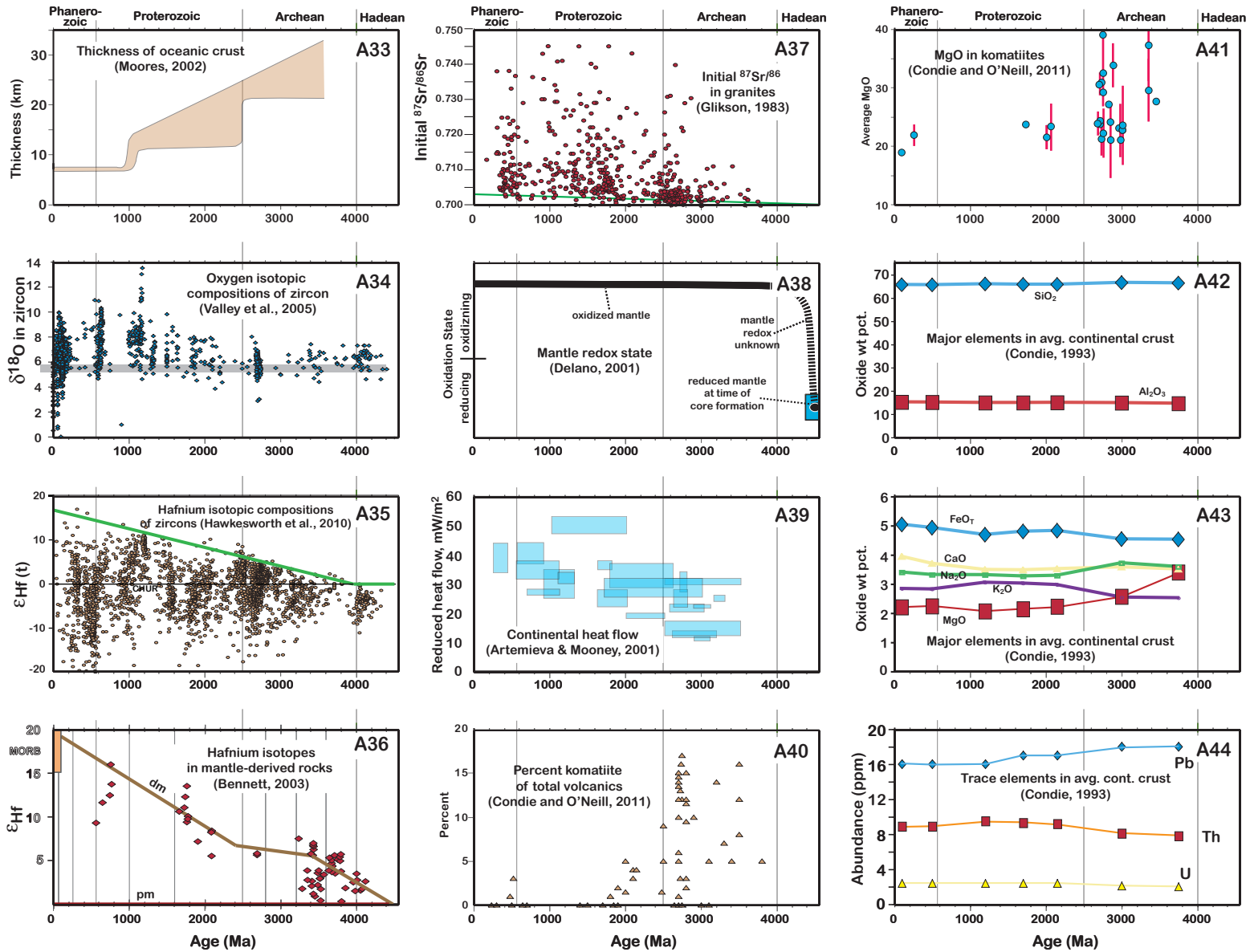
Bradley, Figures A1-A12



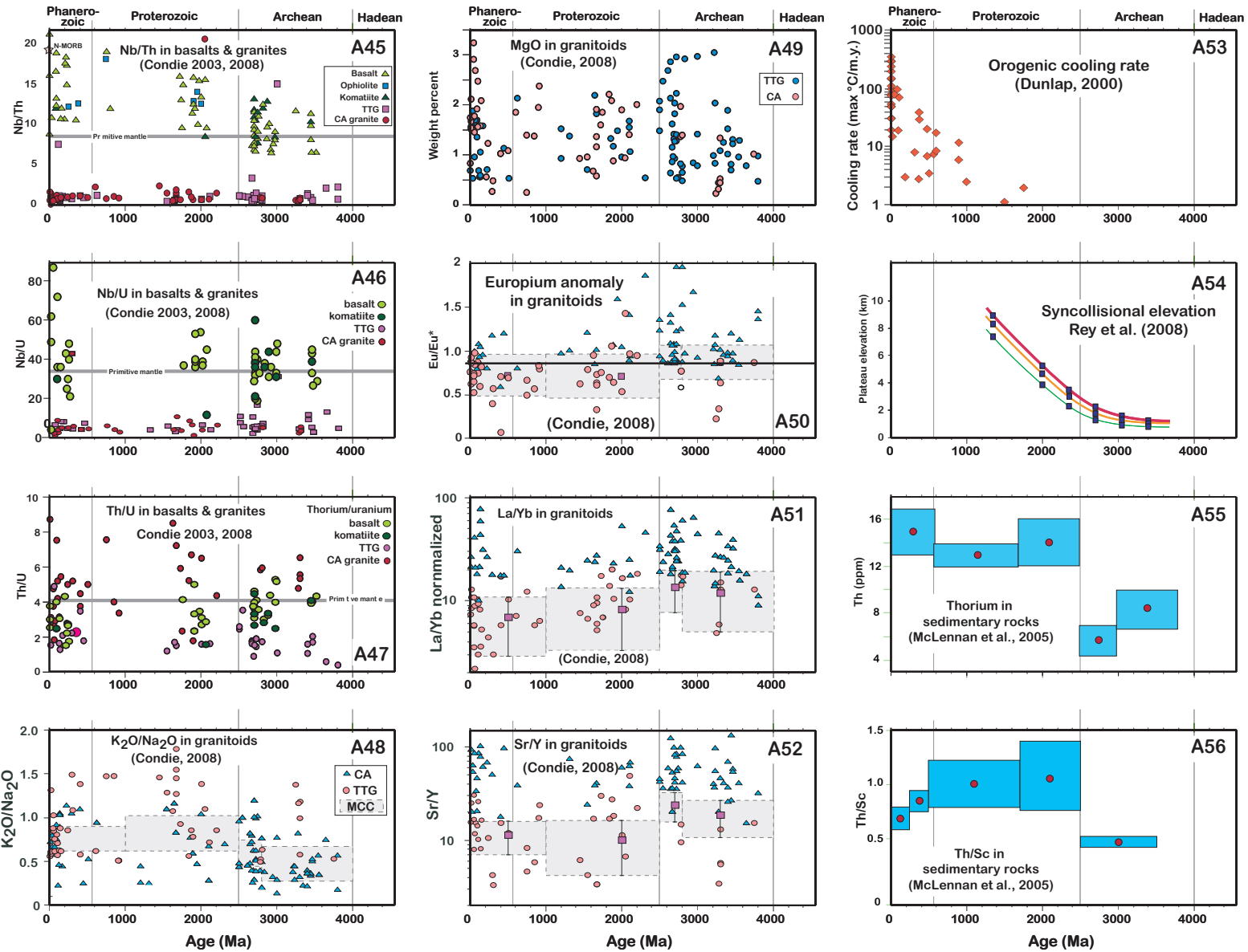
Bradley, Figures A13-A20



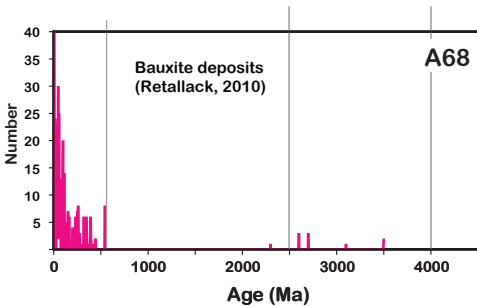
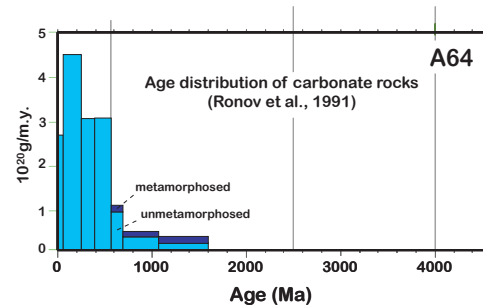
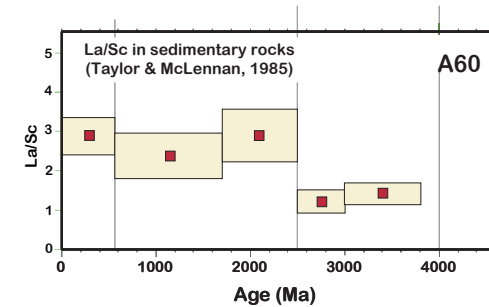
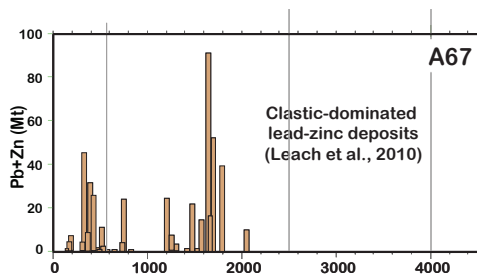
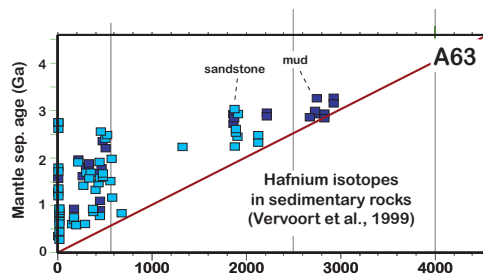
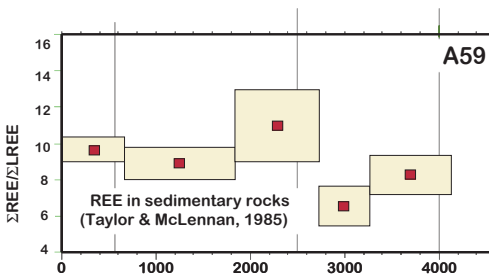
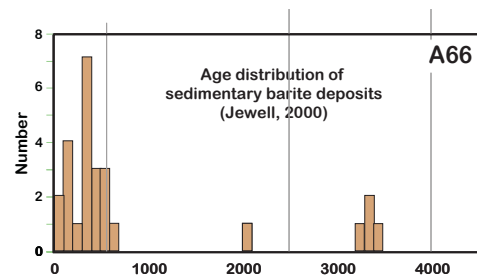
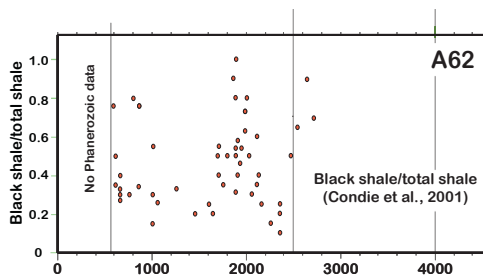
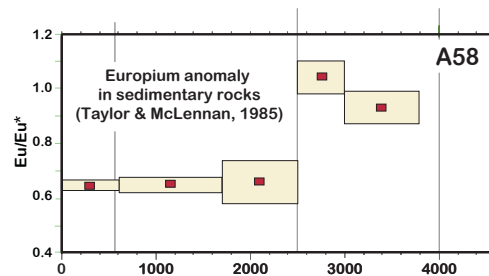
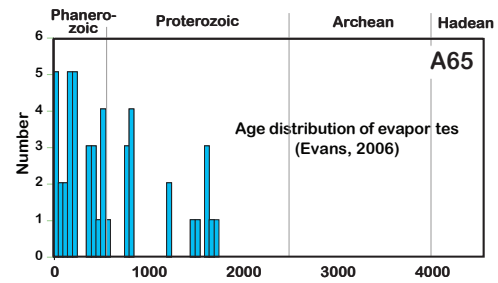
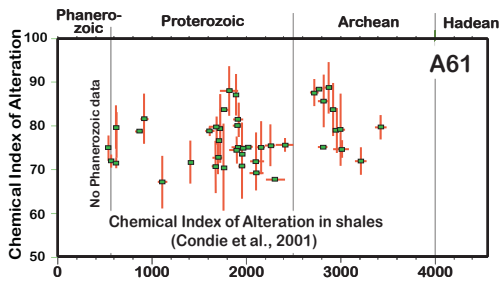
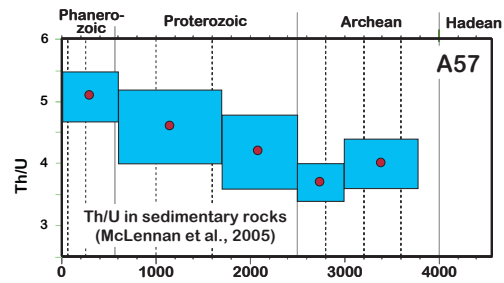
Bradley, Appendix Figures A21-A32

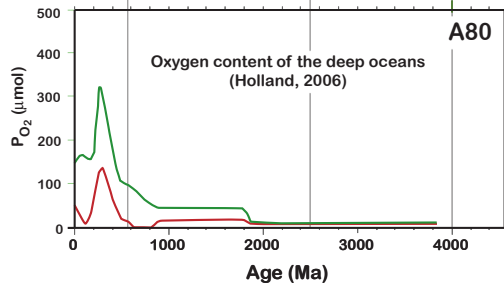
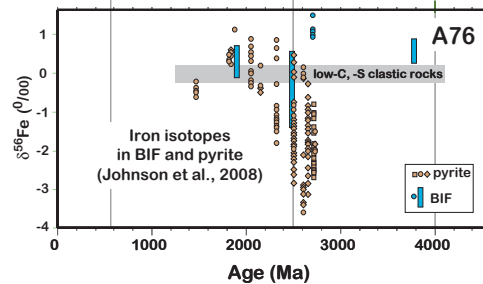
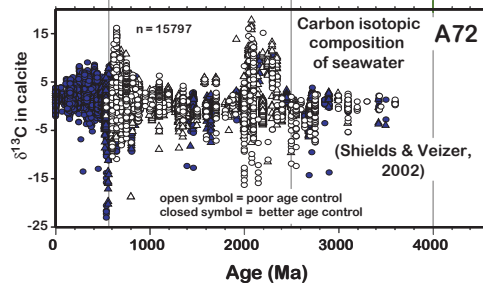
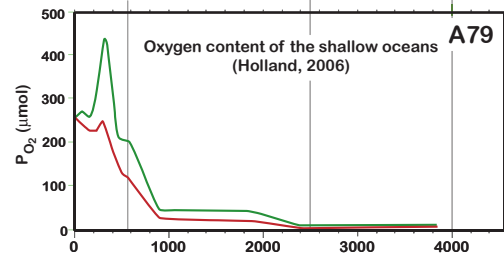
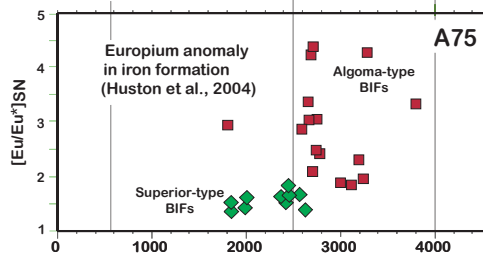
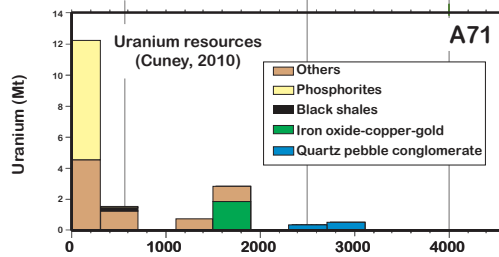
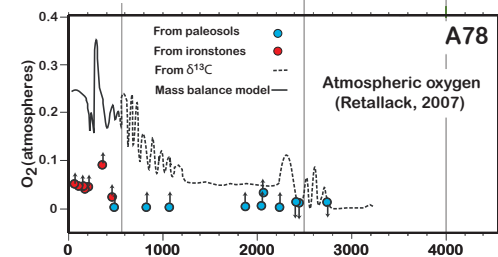
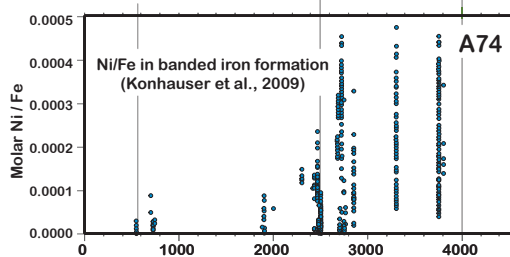
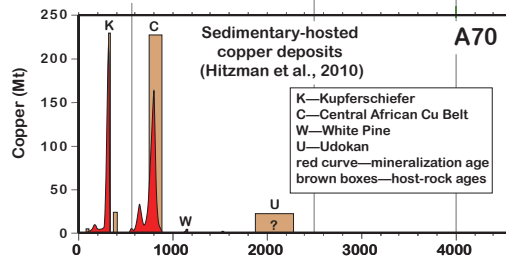
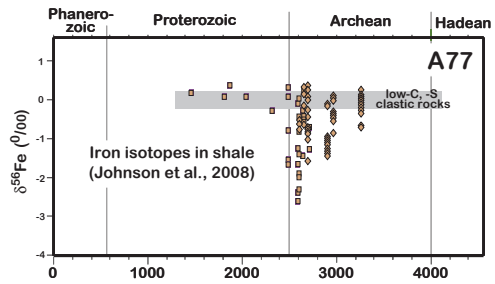
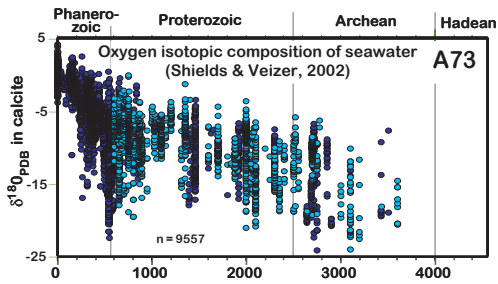
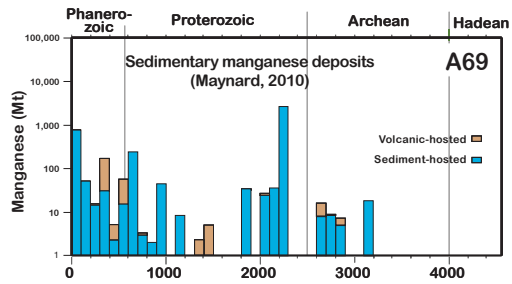


Bradley, Appendix Figures A33-A44



Bradley, Appendix Figures A45 -A56





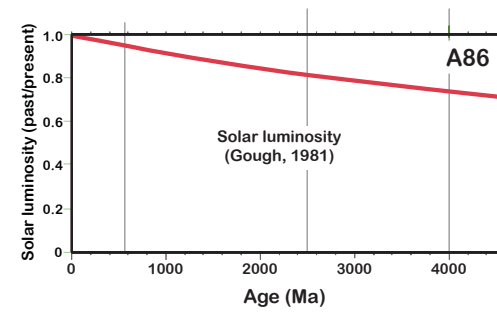
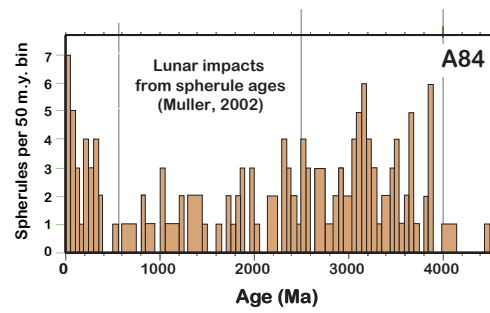
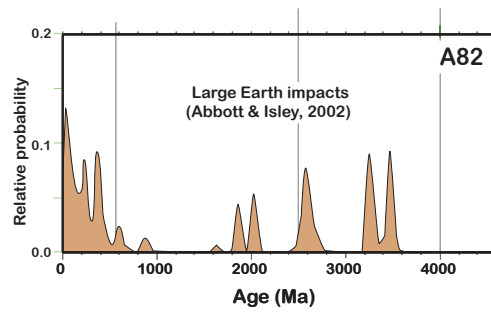
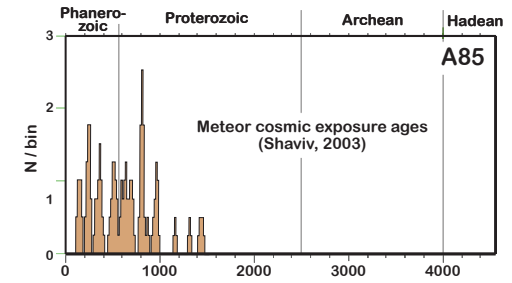
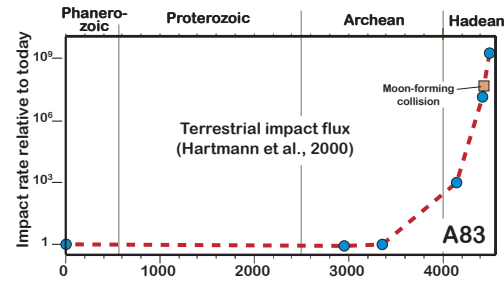
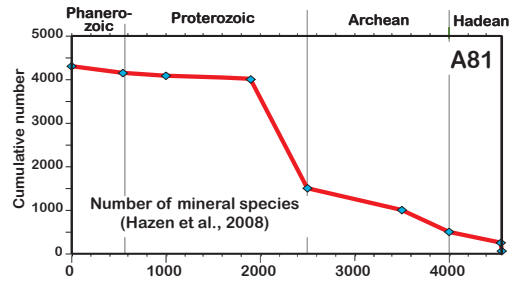


Table A1. Summaries of time-series plots in Figures A1-A86.

Fig. no.	Variable	Time span (Ma)	Reference and comments
A1	Age distribution of volcanic-hosted massive sulfide deposits	0-550	Bekker et al. (2010)
A2	Age distribution of blueschist and ultra-high-pressure metamorphic rocks	0-550	Brown (2007)
A3	Age distribution of sedimentary carbonates	0-550	Mackenzie and Morse (1992)
A4	Calcite to dolomite ratio in sedimentary rocks	0-550	Mackenzie and Morse (1992)
A5	Mineralogy of reef limestones	0-550	Veizer and Mackenzie (2003)
A6	Mineralogy of oolitic limestones	0-550	Morse and Mackenzie (1990)
A7	Age distribution of oolitic limestone	0-550	Wilkinson et al. (1985)
A8	Age distribution of oolitic marine ironstones	0-550	Bekker et al. (2010)
A9	Age distribution of evaporites	0-550	Holser (1984)
A10	Present day halite mass	0-550	Hay et al. (2006)
A11	Reconstructed halite mass	0-550	Hay et al. (2006)
A12	Age distribution of coal	0-550	Orem and Finkelman (2007)
A13	Age distribution of oil source rocks	0-550	Bois et al. (1982)
A14	Phanerozoic seawater chemistry $MgSO_4$ and $CaCl_2$	0-550	Lowenstein et al. (2004)
A15	Strontium concentrations in biological low magnesium calcite	0-550	Veizer and Mackenzie (2003).
A16	Carbon isotopic composition of seawater	0-550	Shields and Veizer (2002)
A17	Oxygen isotopic composition of seawater	0-550	Shields and Veizer (2002)
A18	Sulfur isotopic composition of seawater	0-550	Shields and Veizer (2002). Gray boxes represent data from marine evaporites.
A19	Fossil diversity	0-550	Rohde and Muller (2005)
A20	Minimum latitude of continental glaciation	0-550	Sundquist and Visser (2003)
A21	Age distribution of orogenic granites (old version)	0-4560	Condie (1997)
A22	Rb-Sr ages of granites	0-4560	Glikson (1983)
A23	Detrital zircons from modern river sands	0-4560	Rino et al. (2008)

A24	Pegmatites	0-4560	Tkachev (2011)
A25	Age distribution of greenstone belts	0-4560	Condie (1994)
A26	Age distribution of volcanic-hosted massive sulfide deposits	0-4560	Huston et al. (2010)
A27	Juvenile crust	0-4560	Condie (2005)
A28	Continental growth curves	0-4560	Komiya (2007); see caption to his Figure 14 for references
A29	Thickness of continental crust	0-4560	Durrheim & Mooney (1994)
A30	Mineralogy of subcontinental lithospheric mantle	0-4560	Griffin et al. (2003)
A31	Major elements in subcontinental lithospheric mantle	0-4560	Poudjom Djomani et al (2001)
A32	Thickness of continental lithosphere	0-4560	Artemieva and Mooney (2002)
A33	Thickness of oceanic crust	0-4560	Moore (2003)
A34	Oxygen isotopic compositions of zircons	0-4560	Valley et al. (2005)
A35	Hafnium isotopic compositions of zircons	0-4560	Hawkesworth et al. (2010). The green curve represents depleted mantle.
A36	Hafnium isotopes in mantle-derived rocks	0-4560	Bennett (2003)
A37	Initial $^{87}\text{Sr}/^{86}\text{Sr}$ in granites	0-4560	Glikson (1983)
A38	Mantle redox state	0-4560	Delano (2001)
A39	Continental heat flow	0-4560	Artemieva and Mooney (2001)
A40	Percent komatiite of total volcanics	0-4560	Condie and O'Neill (2011), after de Wit and Ashwal (1997)
A41	MgO in komatiites	0-4560	Condie and O'Neill (2011)
A42	Major elements in avg. continental crust 1	0-4560	Condie (1993)
A43	Major elements in avg. continental crust 2	0-4560	Condie (1993)
A44	Trace elements in avg. continental crust	0-4560	Condie (1993)
A45	Nb/Th in basalts and granites	0-4560	Condie (2003b, 2008)
A46	Nb/U in basalts and granites	0-4560	Condie (2003, 2008)
A47	Th/U in basalts and granites	0-4560	Condie (2003, 2008)
A48	$\text{K}_2\text{O}/\text{Na}_2\text{O}$ in granitoids	0-4560	Condie (2008)
A49	MgO in granitoids	0-4560	Condie (2008)
A50	Europium anomaly in granitoids	0-4560	Condie (2008)
A51	La/Yb in granitoids	0-4560	Condie (2008)
A52	Sc/Y in granitoids	0-4560	Condie (2008)

A53	Orogenic cooling rate	0-4560	Dunlap (2000)
A54	Syncollisional elevation	0-4560	Rey and Coultice (2008)
A55	Thorium in sedimentary rocks	0-4560	McLennan et al. (2005)
A56	Th/Sc in sedimentary rocks	0-4560	McLennan et al. (2005)
A57	Th/U in sedimentary rocks	0-4560	McLennan et al. (2005)
A58	Europium anomaly in sedimentary rocks	0-4560	Taylor and McLennan (1985)
A59	REE in sedimentary rocks	0-4560	Taylor and McLennan (1985)
A60	La/Sc in sedimentary rocks	0-4560	Taylor and McLennan (1985)
A61	Chemical Index of Alteration in shales	0-4560	Condie et al. (2001)
A62	Black shale/total shale	0-4560	Condie et al. (2001)
A63	Hafnium isotopes in sedimentary rocks	0-4560	Vervoort et al. (1999)
A64	Age distribution of carbonate rocks	0-4560	Ronov et al. (1991)
A65	Age distribution of evaporites	0-4560	Evans (2006)
A66	Age distribution of sedimentary barite deposits	0-4560	Jewell (2000)
A67	Clastic dominated lead-zinc deposits	0-4560	Leach et al. (2010)
A68	Bauxite deposits	0-4560	Retallack (2010), who presented a similar plot for laterites, along with detailed time series for 0-300 Ma for both
A69	Sedimentary manganese deposits	0-4560	Maynard (2010)
A70	Sediment-hosted copper deposits	0-4560	Hitzman et al. (2010)
A71	Uranium resources	0-4560	Cuney (2010)
A72	Carbon isotopic composition of seawater	0-4560	Shields and Veizer (2002)
A73	Oxygen isotopic composition of seawater	0-4560	Shields and Veizer (2002)
A74	Ni/Fe in banded iron formation	0-4560	Konhauser et al. (2009)
A75	Europium anomaly in iron formation	0-4560	Huston and Logan (2004)
A76	Iron isotopes in BIF and pyrite	0-4560	Johnson et al. (2008)
A77	Iron isotopes in shale	0-4560	Johnson et al. (2008)
A78	Atmospheric oxygen	0-4560	Retallack (2007)
A79	Oxygen content of the shallow oceans	0-4560	Huston et al. (2004)
A80	Oxygen content of the deep oceans	0-4560	Huston et al. (2004)

A81	Number of mineral species	0-4560	Hazen et al. (2008)
A82	Large Earth impacts	0-4560	Abbott and Isley (2002)
A83	Terrestrial impact flux	0-4560	Hartmann et al. (2000)
A84	Lunar impacts from spherule ages	0-4560	Muller (2002)
A85	Meteor cosmic exposure ages	0-4560	Shaviv (2003)
A86	Solar luminosity	0-4560	Gough (1981)